A Numerical Experiment on Chandrasekhar's Discrete-Ordinate Method for Radiative Transfer: Applications to Cloudy and Hazy Atmospheres[1]

KUO-NAN LIOU

Dept. of Atmospheric Sciences, University of Washington, Seattle 98195

(Manuscript received 19 March 1973, in revised form 18 June 1973)

ABSTRACT

The discrete-ordinate method for radiative transfer introduced originally by Chandrasekhar has been theoretically developed and numerically verified for use in solving the transfer of both solar and thermal infrared radiation through cloudy and hazy atmospheres. This method differs from other radiative transfer approaches in the sense that the solution of the transfer equation can be explicitly derived by employing a finite set of discrete-streams representing the emergent angles in the integral term. Hence such a method is practical for deriving a simplified but reliable radiative transfer approximation for meteorological applications involving clouds and aerosols. Comprehensive comparisons with other rigorous means are carried out for the transmitted and reflected intensity and flux associated with isotropic, Rayleigh and anisotropic scattering. The comparisons reveal that close agreement of radiation computations can be achieved by using discrete-streams of 16. For flux calculations, it was found that values obtained by discrete-streams of 4 yield an accuracy of about 1% for typical phase functions of clouds and haze in either solar or IR radiation, whereas the method of discrete-streams of 2 introduces errors on the order of 3–10%. The solutions for these two simplified cases can be expressed analytically.

Applications have been made by employing wavelengths of 0.7, 1.5 and 10 μm to denote the transfer of solar and thermal IR irradiance through cloudy and hazy atmospheres. For solar radiation, the reflection (albedo), transmission and absorption are obtained as functions of the zenith angle and optical thickness. It is shown that a single-scattering albedo of 0.99 produces absorption of about 30% for a cloud with an optical thickness of 20, and subsequently decreases the albedo by about 20%. The dependence of the transmitted and reflected infrared radiation on the temperatures of particulate layers and ground is illustrated for a number of thicknesses. A cloud at a temperature of −10C would normally reduce the outgoing radiation by about 40%. Interference effects due to thin haze appear to be unimportant. In addition, the net flux and the heating and cooling rates within cloud layers are presented for wavelengths of 1.5 and 10 μm. For a cloud 1 km in thickness, the solar heating takes place near the upper portion at a rate of about 0.3C hr^{-1} μm^{-1} at normal incidence, while it experiences base-warming and top-cooling at a comparable rate resulting from the thermal IR radiation. Although monochromatic wavelengths are used in this study, the method can be extended to include the entire solar and infrared spectrum.

1. Introduction

Improved knowledge of the transfer of solar and terrestrial radiation in the atmosphere, including the influence of clouds and aerosols which occupy regularly at least 50% of the space on a global scale, is of vital importance in the studies of the radiative heat balance, the interaction between radiation and dynamics, and problems related to the remote sensing of atmospheric structure and composition.

Sensing of the atmosphere primarily involves the interpretation of radiometric data which may be recorded according to the region of the electromagnetic spectrum. In the IR region, an excellent example would be the atmospheric temperature profiles derived from the spectral radiation measurement by orbiting meteorological satellites. Such information, however, is greatly hampered by cloud interference. Hence, it is extremely important to obtain a better knowledge of the effects of clouds on the outgoing radiation. Moreover, theoretical evaluations of the distributions of the reflected and transmitted solar irradiance in different cloudy and hazy model atmospheres would certainly provide a valuable basis for the development of remote sensing techniques for probing the macro- and microstructures and composition of clouds and aerosols.

In order to construct a realistic radiative heat balance model for the earth-atmosphere system on a global scale, it is necessary to take the effects of clouds and aerosols into consideration, since the solar heating and IR cooling in cloudy and hazy atmospheres represent one of the initial sources which drive the planetary atmosphere. While the transfer of solar and IR radiation enter their contributions principally in the diabatic heating term of the thermodynamic equation and interrelate with the latent and convective transfer of heat (see, e.g., Dutton and Johnson, 1967), they

[1] Contribution No. 284, Department of Atmospheric Sciences, University of Washington.

depend crucially upon the atmospheric composition, particularly cloudiness and aerosol distributions whose change with time, in turn, rely on the dynamic conditions. With such a complicated feedback mechanism, namely, the interaction of the incoming and outgoing radiation with the kinematic dynamics, a more comprehensive understanding of the radiative heat transfer in cloudy and hazy atmospheres for different time scales undoubtedly would provide an improvement in global numerical weather prediction.

The formal solutions for the transfer of radiation have been elegantly derived by Chandrasekhar (1950) who was mainly concerned with astrophysical applications. Following Sekera's efforts (1956), such sophisticated mathematical formulations have been applied to many meteorological problems, noticeably the scattering and polarization in Rayleigh atmospheres, resulting in a set of valuable tables (Coulson *et al.*, 1960). Hence the problem of scattered radiation in clear atmospheres appeared to have been completely solved. Since then, progress has been made in the investigations of the transfer of solar and thermal IR radiation through cloudy and hazy atmospheres. After van de Hulst (1963) had outlined a numerical procedure for multiple scattering from a plane-parallel atmosphere (known as the doubling method), numerical computations and additional theories including polarization were developed (e.g., Twomey *et al.*, 1966; van de Hulst and Grossman, 1968; Irvine, 1968; Hunt and Grant, 1969; Hansen, 1969; Howell and Jacobowitz, 1970; Hovenier, 1969, 1971; Hansen, 1971a,b). Other radiative transfer techniques include the Monte Carlo method used most productively by Plass and Kattawar (1971) and Danielson *et al.* (1969), the Gauss-Seidel scheme developed by Herman and Browning (1965) and extended to cases of polarization by Dave (1970) and Herman *et al.* (1971), and the invariant imbedding method employed by Bellman *et al.* (1966).

To achieve certain accuracy in the intensity and flux calculations with the above techniques, considerable amounts of computer time are frequently required and the computations are generally carried out by successively iterative numerical means. Moreover, these numerical methods have been mainly concerned with the radiation field on the boundaries of the atmospheres. Hardly any schemes have been engaged with the evaluations of the internal radiation field which is closely associated with the heating and cooling rates of the scattering layers, and therefore related to the stability of clouds and haze. In order to calculate the internal radiation of a scattering layer, additional computer time and numerical procedures have to be employed.

For many meteorological applications the development of a simplified method for treating radiation in the solar and terrestrial spectrum seems to be highly desirable. Such a method should take into account the distribution, thickness and type of clouds and aerosols. Along these lines, Atwater (1971) has used the single-scattering approximation to study the pollutant effects on the radiative balance in atmospheric boundary layers. Shettle and Weinman (1970) have developed a simple method based upon the Eddington's approximation which takes two terms in the expansion of phase functions. With a similar approach, Samuelson (1970) and McElroy (1971) have employed a 2-points Gaussian quadrature to investigate non-local thermodynamic equilibrium and absorption line formation in a scattering atmosphere, respectively. Weinman and Geutter (1972) have further extended to a 4-points quadrature using a Henyey-Greenstein analytic phase function to study the solar irradiance penetrating into a plant canopy. Liou (1973) has also developed a simplified method with the assumption made only in the integral form of the radiative transfer equation to investigate the transfer of solar irradiance through cirrus cloud layers.

Despite all the above approximate methods which in certain cases do yield satisfactory results, it is felt that a more inclusive means of determining radiative transfer should be developed. Thus, if radiation computations were to be performed on both global space and time scales, the theory of radiative transfer might just have to be parameterized somehow. The discrete-ordinate method for radiative transfer, introduced originally by Chandrasekhar, was thought to be, perhaps, one of the most potential means for serving such purposes, because the solutions of the integral-differential transfer equation can be explicitly derived. Efforts have therefore been concentrated on exploring the usefulness and applicability of this method for radiation studies in cloudy and hazy atmospheres. It has been previously discussed by Piotrowski (1956) for conservative scattering, and Samuelson (1967, 1969) and Yamamoto *et al.* (1971) have used it in the studies of IR radiation. Keller (1958, 1960a, b) has discussed extensively the problems of convergence especially for isotropic scattering. Lenoble (1956) has also made certain contributions.

We first present theoretical analyses of the discrete-ordinate method for both solar and thermal IR radiation, and then discuss certain problems and shortcuts in the computational procedures. Next, in order to demonstrate the validity of the method, a number of quantitative verifications are given by comparison with other established computations. Finally, illustrations of several applications to cloudy and hazy atmospheres are carried out by employing monochromatic wavelengths of 0.7 and 1.5 μm to represent cases for solar radiation, and 10 μm for IR radiation. These applications contain the reflected and transmitted intensity, the reflection and transmission in the form of flux, the absorption of solar irradiance, as well as the net flux and the heating and cooling rates within the cloud and haze layers.

2. The discrete-ordinate method for radiative transfer

The spectrum distribution of electromagnetic energy emitted by the sun, assuming a temperature of ~6000K, generally covers the wavelength band from ~0.1 to ~3 μm, with maximum intensity at ~0.47 μm. On the other hand, the terrestrial radiation from the earth, assuming a temperature of ~250K, emits energy over the wavelength band from ~5 to ~100 μm with maximum intensity at ~12 μ. Since at a temperature of ~250K radiation of wavelengths $\leqslant 4$ μm is of negligible energy, and since the solar flux carries little energy at greater wavelengths, it is convenient to treat the solar and thermal IR radiation separately to avoid any possible complications. Accordingly, we shall divide the theoretical developments of the discrete-ordinate method for radiative transfer into two parts.

a. Solar radiation

The basic equation describing the diffuse intensity of solar radiation can be written (Chandrasekhar, 1950)

$$\mu\frac{dI(\tau,\mu,\phi)}{d\tau}=I(\tau,\mu,\phi)-\frac{1}{4\pi}\int_0^{2\pi}\int_{-1}^{+1}p(\mu,\phi;\mu',\phi')\times I(\tau,\mu',\phi')d\mu'd\phi'-\tfrac{1}{4}F_0p(\mu,\phi;\mu_0,\phi_0)\exp(-\tau/\mu_0), \quad (1)$$

where I represents the intensity, τ the optical thickness, F_0 the incident solar flux, and μ and μ_0 the cosine of the emergent and solar zenith angles, respectively. From the spherical geometry, the relationships between the scattering angle Θ, the cosine of zenith angles μ, μ', and the azimuth angles ϕ, ϕ' can be derived. Hence, by the addition theorem of spherical harmonics (see, e.g., Stratton, 1941), the phase function p can be expanded in Legendre polynomials P_l consisting of a finite number of terms as

$$p(\mu,\phi;\mu',\phi')=\sum_{m=0}^{N}(2-\delta_{0,m})\Big[\sum_{l=m}^{N}\tilde{\omega}_l\overset{m}{P}_l(\mu)\overset{m}{P}_l(\mu')\Big]\times\cos m(\phi'-\phi), \quad l=m,\ldots,N, 0\leqslant m\leqslant N, \quad (2)$$

with

$$\tilde{\omega}_l=\tilde{\omega}_l\frac{(l-m)!}{(l+m)!}, \qquad \delta_{0,m}=\begin{cases}1, & \text{if } m=0\\ 0, & \text{otherwise}\end{cases}$$

where $\tilde{\omega}_l$ $(l=0,1,\ldots,N)$ are a set of $N+1$ constants which can be determined by noting the orthogonal property of the Legendre polynomials. The $\tilde{\omega}_0$ denotes the well-known single-scattering albedo and $\tilde{\omega}_1/3\tilde{\omega}_0=\langle\cos\Theta\rangle$ represents the asymmetry factor.

Substituting (2) into (1), and noting that the intensity $I(\tau,\mu,\phi)$ may also be expanded in a cosine series such that

$$I(\tau,\mu,\phi)=\sum_{m=0}^{N}I^m(\tau,\mu)\cos m(\phi_0-\phi), \quad (3)$$

we obtain (after making some algebraic rearrangements) $N+1$ independent equations of

$$\mu\frac{dI^m(\tau,\mu)}{d\tau}=I^m(\tau,\mu)-\tfrac{1}{2}\sum_{l=m}^{N}\tilde{\omega}_l\overset{m}{P}_l(\mu)\int_{-1}^{+1}\overset{m}{P}_l(\mu')I^m(\tau,\mu')d\mu'-\tfrac{1}{4}F_0(2-\delta_{0,m})\Big[\sum_{l=m}^{N}\tilde{\omega}_l(-1)^{m+l}\overset{m}{P}_l(\mu)\overset{m}{P}_l(\mu_0)\Big]\times\exp(-\tau/\mu_0), \quad m=0,1,2,\ldots,N, \quad (4)$$

where the factor $(-1)^{m+l}$ in the last term indicates that the solar irradiance is pointing downward. On the nth approximation for the discrete-ordinate method, the integral in Eq. (4) is to be replaced by the sums according to the Gauss's quadrature formula by placing on the interval $-1\leqslant\mu\leqslant 1$ a set of $2n(n\neq 0)$ points μ_j and weights a_j obtained from $P_{2n}(\mu)=0$ and Gauss's formula, respectively. Thus, with the integral replaced by the summation, we obtain the following $2n$ first-order, nonhomogeneous differential equations for given m as

$$\mu_i\frac{dI^m(\tau,\mu_i)}{d\tau}=I^m(\tau,\mu_i)-\tfrac{1}{2}\sum_{l=m}^{N}\tilde{\omega}_l\overset{m}{P}_l(\mu_i)\sum_j a_jI^m(\tau,\mu_j)\overset{m}{P}_l(\mu_j)-\tfrac{1}{4}F_0(2-\delta_{0,m})\Big[\sum_{l=m}^{N}(-1)^{l+m}\tilde{\omega}_l\overset{m}{P}_l(\mu_i)\overset{m}{P}_l(\mu_0)\Big]\times\exp(-\tau/\mu_0), \quad i(-n,+n),\ 0\leqslant m\leqslant N, \quad (5)$$

where $\sum_j$ denotes that j runs from $-n$ to n, and $j\neq 0$. Since the maximum order of polynomial expansions N exists under the integral which was changed to sums according to Gauss's quadrature weights, it should be noted that the expanded terms of Legendre polynomials should not exceed $2n$.

Since we are primarily interested in the azimuth-independent cases of solar radiation in cloudy and hazy atmospheres, we shall consider the first term of the intensity expansion ($m=0$) in Eq. (3). Dropping the superscript 0, the equations for the diffuse intensity reduce to the form

$$\mu_i\frac{dI(\tau,\mu_i)}{d\tau}=I(\tau,\mu_i)-\tfrac{1}{2}\sum_{l=0}^{N}\tilde{\omega}_lP_l(\mu_i)\sum_j a_jP_l(\mu_j)I(\tau,\mu_j)-\tfrac{1}{4}F_0\Big[\sum_{l=0}^{N}(-1)^l\tilde{\omega}_lP_l(\mu_i)P_l(\mu_0)\Big]\exp(-\tau/\mu_0). \quad (6)$$

The simultaneous solutions for the above $2n$ differential equations can be derived from the procedures briefly

illustrated below: First, we look for the general solutions for the associated homogeneous system in Eq. (6). Following the analyses given by Chandrasekhar (1950), the intensity at each discrete Gaussian point may be assumed as

$$I(\tau,\mu_i)=\frac{\exp(-k\tau)}{1+\mu_i k}\sum_{l=0}^{N}\tilde{\omega}_l\xi_l P_l(\mu_i), \tag{7}$$

where the k's denote the eigenvalues corresponding to the associated homogeneous differential equations. They may physically be explained as some sort of extinction coefficients. The ξ_l represent certain proportional constants which can be determined by substituting (7) into (6). With some mathematical manipulations, it can be shown that

$$\xi_{l+1}=-\frac{2l+1-\tilde{\omega}_l}{k(l+1)}\xi_l-\frac{l}{l+1}\xi_{l-1},\quad l=0,1,\ldots,N-1. \tag{8}$$

Since the ξ_l are proportional constants, the simplest (and arbitrary) choice is that of setting $\xi_0=1$. Thus, all ξ_l may then be evaluated with a simple iterative scheme. In addition, by substituting (7) into (6), we also obtain the characteristic equation for searching the eigenvalues, i.e.,

$$\xi_\lambda(k_j)=\tfrac{1}{2}\sum_i a_i P_\lambda(\mu_i)W_j(\mu_i), \tag{9}$$

where

$$W_j(\mu_i)=\frac{1}{1+\mu_i k_j}\sum_{l=0}^{N}\tilde{\omega}_l\xi_l(k_j)P_l(\mu_i). \tag{10}$$

By selecting $\xi_0(k_j)=1$ in Eq. (8), we get one equation which consists of all the eigenvalues required for Eq. (6). We shall call the above procedure Chandrasekhar's method for determining the eigenvalues in the discrete-ordinate method for radiative transfer. In view of Eqs. (8)–(10), we shall have $2n+N$ values for k when N is an even number, and $2n+N-1$ values when N is odd. Hence, the eigenvalues must occur in pairs (i.e., $k_j=-k_{-j}$). A comprehensive discussion concerning the problems of seeking the eigenvalues based upon Eq. (9) [with $\xi_0(k_j)=1$] will be given in the section of numerical procedures.

Now, we shall add a particular solution for the non-homogeneous system to complete the problem. It can be shown that

$$I_p(\tau,\mu_i)=Z(\mu_i)\exp(-\tau/\mu_0), \tag{11}$$

where

$$Z(\mu_i)=\tfrac{1}{4}\mu_0 F_0\frac{H(\mu_0)H(-\mu_0)}{\mu_0+\mu_i}\sum_{l=0}^{N}\tilde{\omega}_l\xi_l\left(\frac{1}{-\mu_0}\right)P_l(\mu_i), \tag{12}$$

satisfies Eq. (6). The H function for an argument of μ in the nth approximation (Chandrasekhar, 1950, Chap. 5) is

$$H(\mu)=\frac{1}{\mu_1\mu_2\cdots\mu_n}\prod_{i=1}^{n}(\mu+\mu_i)\Big/\prod_{j=1}^{n}(1+k_j\mu). \tag{13}$$

Thus, the complete simultaneous solutions for the integral-differential transfer equation in the nth approximation with the $2n$ undetermined coefficients denoted as L_j can be written as

$$I(\tau,\mu_i)=\sum_j L_j W_j(\mu_i)\exp(-k_j\tau)+Z(\mu_i)\exp(-\tau/\mu_0). \tag{14}$$

Eq. (14) is valid only for non-conservative scattering, because for $\tilde{\omega}_0=1$, $k^2=0$ will be values that satisfy the characteristic equation, and hence $\xi_l(k)$ becomes indefinite. Thus, a different solution should be derived. In conservative cases, where there is no absorption, the flux of radiation normal to the plane of stratification is constant. It can be easily shown that the transfer equation admits a solution of the form

$$I(\tau,\mu_i)=\sum_{j=-(n-1)}^{n-1}L_j W_j(\mu_i)\exp(-k_j\tau)+[(1-\tilde{\omega}_1/3)\tau+\mu_i]L_{-n}+L_n+Z(\mu_i)\exp(-\tau/\mu_0), \tag{15}$$

where the second and third terms in the right-hand side are derived from the conservation of fluxes. The boundary conditions describing the diffuse intensity for the solar radiation may be expressed as

$$\left.\begin{aligned} &I(0,-\mu_i)=0\\ &I(\tau_N,\mu_i)=\frac{As}{\pi}\Big[-2\pi\sum_{i=1}^{n}a_i\mu_i I(\tau_N,-\mu_i)+\pi\mu_0 F_0\exp(-\tau_N/\mu_0)\Big]\end{aligned}\right\}, \tag{16}$$

i.e., no downward diffuse intensities at the top of the scattering layer, while the upward diffuse intensities at the bottom of the layer equal the product of the ground albedo (As) and the total downward irradiance reaching the optical depth (τ_N). It should be noted that we use positive and negative discrete points to denote the upward and downward streams of radiation respectively. With the boundary conditions specified above, values of L_j can be numerically evaluated. Hence, the upward and downward intensities may then be calculated from Eqs. (14) or (15) for any given optical thickness τ. Moreover, the reflected and transmitted intensities on the boundary of a scattering layer can be easily obtained. For non-conservative scattering, they are, respectively,

$$I(0,\mu_i)=\sum_j L_j W_j(\mu_i)+Z(\mu_i), \tag{17}$$

$$I(\tau_N, -\mu_i)=\sum_j L_j W_j(-\mu_i)\exp(-k_j\tau_N) + Z(-\mu_i)\exp(-\tau_N/\mu_0). \quad (18)$$

Since similar expressions can be written for conservative scattering, we shall not repeat them here.

b. Thermal infrared radiation

For a plane-parallel layer in local thermodynamic equilibrium with the assumption that the scattering and emitting layer is isothermal, the appropriate transfer equation describing the radiation field may be written

$$\mu\frac{dI_\nu(\tau,\mu)}{d\tau}=I_\nu(\tau,\mu)-\frac{1}{2}\int_{-1}^{+1}p_\nu(\mu,\mu')I_\nu(\tau,\mu')d\mu' -(1-\tilde{\omega}_{0\nu})B_\nu(T), \quad (19)$$

where the axially-symmetrical phase function

$$p(\mu,\mu')=\frac{1}{2\pi}\int_0^{2\pi}p(\mu,\phi;\mu',\phi')d\phi', \quad (20)$$

and the Planck function

$$B_\nu(T)=\frac{2h\nu^3}{c^2}\frac{1}{\exp(h\nu/KT)-1}. \quad (21)$$

In the above equations, T is the isothermal temperature within the scattering layer, the subscript ν denotes the frequency dependence, h and K are known as Planck's and Boltzmann's constants, while c is the velocity of light. The last term in Eq. (19) represents the contributions of the thermal emission from the scattered particulates. As discussed in the previous subsection, the phase function can be expanded in the form of Legendre polynomials with the integral being replaced by sums. By omitting the frequency index on the phase function and the single-scattering albedo for simplicity, we have

$$\mu_i\frac{dI_\nu(\tau,\mu_i)}{d\tau}=I_\nu(\tau,\mu_i)-\tfrac{1}{2}\sum_{l=0}^{N}\tilde{\omega}_l P_l(\mu_i)\sum_j a_j P_l(\mu_j) \times I_\nu(\tau,\mu_j)-(1-\tilde{\omega}_0)B_\nu(T). \quad (22)$$

Because the solutions for the associated homogeneous system are exactly the same as in the case of solar radiation discussed previously, we need only find a particular solution for Eq. (22). It can easily be shown that

$$I_{\nu p}(\tau,\mu_i)=B_\nu(T) \quad (23)$$

satisfies Eq. (22). Therefore, the complete simultaneous solutions for Eq. (22) yield

$$I_\nu(\tau,\mu_i)=\sum_j L_j W_j(\mu_i)\exp(-k_j\tau)+B_\nu(T), \quad i(-n,n). \quad (24)$$

The boundary conditions for thermal IR radiation with contributions from the upper and lower Rayleigh layers may generally be expressed as

$$I_\nu(\tau_t, -\mu_i)=\int_{\tau_t}^{\tau_\infty}B_\nu[T(\tau)] \times\exp[-(\tau-\tau_t)/-\mu_i]d\tau/-\mu_i, \quad (25)$$

$$I_\nu(\tau_b,\mu_i)=B_\nu(T_g)\exp(-\tau_b/\mu_i)+\int_0^{\tau_b}B_\nu[T(\tau)] \times\exp[-(\tau_b-\tau)/\mu_i]d\tau/\mu_i, \quad (26)$$

where τ_t and τ_b $[=\tau_t-\tau_N]$ are the optical thicknesses from the earth's surface to the top and the bottom of the scattering layer, respectively, and T_g is the ground temperature. From the above two equations, the coefficients L_j may hence be obtained. Thus, for any given optical thickness of τ, the intensity of the thermal infrared radiation can be evaluated. Furthermore, the reflected and transmitted intensities are

$$I_\nu(0,\mu_i)=\sum_j L_j W_j(\mu_i)+B_\nu(T), \quad (27)$$

and

$$I_\nu(\tau_N, -\mu_i)=\sum_j L_j W_j(-\mu_i)\exp(-k_j\tau_N)+B_\nu(T). \quad (28)$$

At this point, we have discussed all the necessary mathematical analyses for the discrete-ordinate method for the transfer of either solar or thermal IR radiation through a multiply-scattered particulate layer. Finally, the upward and downward fluxes for any given τ in both cases are

$$\left.\begin{aligned}F\uparrow(\tau)&=2\pi\sum_{i=1}^{n}a_i\mu_i I(\tau,\mu_i)\\ F\downarrow(\tau)&=-2\pi\sum_{i=1}^{n}a_i\mu_i I(\tau,-\mu_i)-s(\tau,-\mu_0)\end{aligned}\right\}, \quad (29)$$

where

$$s(\tau,-\mu_0)=\begin{cases}\pi\mu_0 F_0\exp(-\tau/\mu_0), & [\text{SOL}]\\ 0, & [\text{IR}]\end{cases}$$

The symbols SOL and IR denote the solar and terrestrial radiation respectively.

3. Numerical procedures

We have developed the theoretical basis for the discrete-ordinate method for both solar and thermal IR radiation. We shall now proceed to discuss, in order, the problems and some shortcuts for numerical computations.

a. Expansion of phase functions

Computations of phase functions, which indicate the distribution of the monochromatic scattered energy for

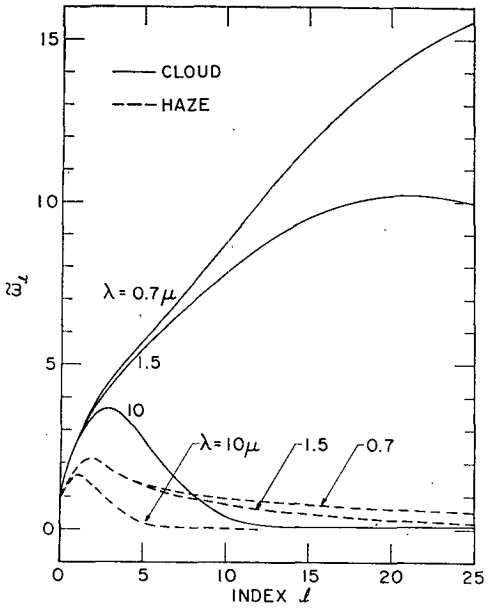

FIG. 1. The coefficients $\tilde{\omega}_l$ in the Legendre polynomial expansions of the phase functions for clouds and haze.

single scattering typical for clouds and hazes were made at wavelengths of 0.7, 1.5 and 10 μm. They will be presented and discussed in Section 5. Here, let us assume that phase functions are given as functions of the scattering angle, so that they can then be expanded in the form of Legendre polynomials according to Eq. (2). By means of any standard integration technique, the coefficients $\tilde{\omega}_l$ of the polynomials can be evaluated for any index l. The first one $\tilde{\omega}_0$ represents the well-known single-scattering albedo, which is always normalized to unity for the purpose of graph presentations.

It was known that for isotropic and Rayleigh scattering, the expansions of Legendre polynomials yield one and three (with the second term being zero) terms, respectively. To obtain some quantitative values with respect to anisotropic scattering for both clouds and hazes, results of $\tilde{\omega}_l$ were plotted as functions of the index l (Fig. 1). The scattered energy from clouds in the visible and near-IR concentrates primarily in the forward directions and consists of several features such as cloud bows and glory; consequently, to describe more precisely such complicated and sharp phase functions more terms of $\tilde{\omega}_l$ are needed as illustrated in cases where $\lambda=0.7$ and 1.5 μm. For hazes, there are no sharp diffraction peaks because the sizes of aerosols are much smaller. The values of $\tilde{\omega}_l$ for $l \gtrsim 10$ are all less than unity. It should also be noted that the imaginary parts of the refractive index used are 0.001 and 0.01 for $\lambda=0.7$ and 1.5 μm, respectively. For $\lambda=10$ μm, where there is large absorption by particles in both clouds and hazes, obviously only a few terms are necessary to describe the phase functions.

In the discrete-ordinate method, since the Legendre polynomials of maximum N occur under the integral sign which was replaced by the approximated sums of $2n$ terms, the expansions of N should not exceed the discrete points of $2n$. Physically speaking, increasing the terms of polynomials beyond N will not improve the accuracy of the method. In order to obtain the maximum accuracy of the results, we have used $N=2n-1$ throughout this investigation.

After the coefficients $\tilde{\omega}_l$ are determined, the next step is to obtain the corresponding eigenvalues for a set of $2n$ homogeneous differential equations.

b. Determination of eigenvalues

In Section 2 we presented the formulas involved in Chandrasekhar's method for searching the eigenvalues corresponding to the $2n$ associated homogeneous differential equations. This method as we will point out later appears to have some mathematical as well as numerical ambiguities. Therefore, we shall explain the problem involved more clearly by explicitly expanding the characteristic equation derived from Eq. (9) as follows:

$$f(k)=1-\sum_{j=1}^{n}\frac{a_j}{1-\mu_j^2k^2}\Big[\sum_{l=0}^{N/2}\tilde{\omega}_{2l}\xi_{2l}(k)P_{2l}(\mu_j) -\mu_j k\sum_{l=0}^{(N-1)/2}\tilde{\omega}_{2l+1}\xi_{2l+1}(k)P_{2l+1}(\mu_j)\Big]. \quad (30)$$

The bracket on the right-hand side of Eq. (30) contains k^{-N} (N, even) or $k^{-(N-1)}$ (N, odd) terms which are produced from the iterative procedures based upon Eq. (8). As a result, in addition to the $2n$ eigenvalues due to the factor of $(1-\mu^2k^2)^{-n}$, we shall have N or $N-1$ eigenvalues which should also occur in pairs. However, mathematically, since there are only $2n$ differential equations, the eigenvalues must not exceed $2n$ values. It would appear, therefore, that the additional values that might be produced from Eq. (30) are probably either all zeros, or cannot be distinguished from the required $2n$ values, or may be complex numbers which are unphysical in the discrete-ordinate method.

Extensive experiments utilizing Eq. (30) for seeking the corresponding eigenvalues have been made so as to investigate the possible ambiguity implicated. It was found that with a sufficient small increment of k, only $2n$ values were obtained numerically for both strong and less strong anisotropic phase functions. In order to explore the possible mathematical and physical reasons stated in the previous paragraph, we have expanded the equation in the form of polynomials for $n=1$ and $n=2$. From the polynomials, we shall be able to obtain the additional eigenvalues. We have discovered that the additional values are all zeros. It follows that all the additional eigenvalues have to be zeros for any order of n.

Besides the ambiguity of the eigenvalues involved by means of the Chandrasekhar's method, a fairly large

amount of computer time is also required to find all of them, especially for large n. With these shortages in mind, a more economical and straightforward means for solving the eigenvalue problem seems to be desirable and necessary. We have developed a method directly from the associated differential equations for the problem of eigenvalues. The mathematical and numerical analyses are given in the Appendix. We shall call this method the "matrix method" for the eigenvalue problem. Since the matrix involved is unsymmetrical, it is felt that the best way to obtain eigenvalues is to expand the matrix in the polynomial form. The matrix method contains no ambiguity in the numbers of eigenvalues, and it takes a very small amount of computer time even for large n (e.g., for discrete-streams of 16, $\sim$10 sec are required in the CDC 6400 computer, while $\sim$3 min are needed using Chandrasekhar's method to obtain the same accuracy).

The matrix method provides eigenvalue accuracies at least up to about seven decimal points for discrete-streams $\lesssim$10. For discrete-streams of 16, which we use extensively in the intensity and flux computations, the accuracy is generally reduced to four or five figures as a result of the high-order matrix multiplications. These were all checked by comparing them with values obtained from the Chandrasekhar method. Having an accuracy of about five decimal points for the eigenvalues (except for the smallest one for large n) ensures rather stable distributions for intensity and flux computations. A discussion of the difficulties produced by the smallest eigenvalues for non-conservative scattering will be given in the following subsection.

Fig. 2 illustrates a typical distribution of eigenvalues for an anisotropic scattering having a single scattering albedo of 0.95. It can be easily understood from Eq. (30) that $f(k_i) \to \pm\infty$, as $k_i \to \mu_i^{-1}$. In this figure, the same intervals between each μ_i^{-1} were divided so that lines across the zeros could be clearly presented. For isotropic scattering, there exists one and only one eigenvalue in each interval (Keller, 1960a). Hence, the anisotropy obviously destroys the symmetry of the characteristic equation. For strong anisotropic scattering where more energy concentrates in the forward directions (i.e., very sharp phase function), more values would lie in the first interval $(0, \mu_n^{-1})$. Three were shown in this demonstration.

c. *Stabilization of the W-function*

The most troublesome problem in the numerical computations of the discrete-ordinate method is the unstable results, especially for the intensity distribution, caused by the smallest eigenvalues (hereafter denoted to as k_s) for discrete-streams $\gtrsim$10. With the accuracy of the eigenvalues k_j up to about five decimal points, the H-functions, the exponential functions, and other terms produce very stable results. The meaning of "stable" is defined here such that an increase in the accuracy of k_j does *not* increase the accuracy of the results to more than about five decimal points. Furthermore, all of the W-functions are also rather stable except those obtained by k_s. As we can see from Eq. (10), W-functions are closely associated with ξ-functions which are evaluated by means of the iterative procedures from Eq. (8), and which increase the inverse power of k. Suppose the value of k_s is very small, typically say $\lesssim$0.2, then the ξ-function will obviously lose its accuracy for large l due to roundoff errors in spite of how precise the numbers the computer could handle. As a result, k_s may produce unstable solutions for ξ-functions and hence for W-functions.

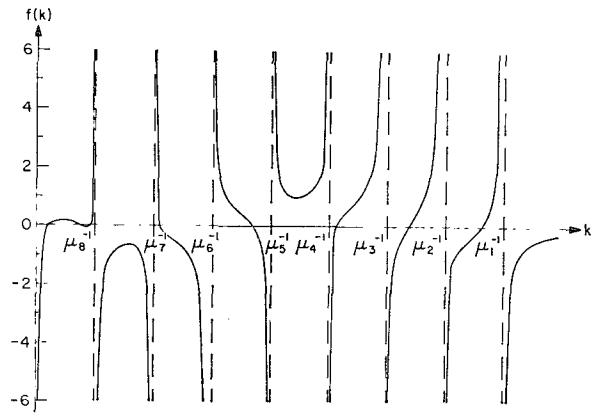

FIG. 2. A typical distribution of eigenvalues for an anisotropic phase function with a single-scattering albedo of 0.95, for equal intervals between each μ_i^{-1}.

In the case of conservative scattering, $k_s = 0$, so no such unstable problems will occur. However, for cases of $\tilde{\omega}_0 \to 1$ or cases of sharp phase functions, the values of k_s are often very small. Thus, even with very accurate values (up to say 10 digits), the ξ-functions and hence the W-functions are frequently unstable. The merit of Chandrasekhar's single equation [Eq. (30)] for obtaining all eigenvalues is essentially based upon the selection of the first ξ-function, namely, assuming $\xi_0(k_j) = 1$ for all j. From such a choice, $\xi_l(k_j)$ for all l and j may therefore be evaluated by a simple iterative scheme. Subsequently, $W_j(\mu_i)$ can then be calculated. Now, by noting the feedback relationships between the ξ- and W-functions from Eqs. (9) and (10), it is understood that values of k_j must satisfy both of them. Except for k_s, the rest of the eigenvalues seem to follow the feedback restrictions with negligible computational errors ($\lesssim 10^{-5}$).

Recognizing the above complications, it was found that the stabilization of the W-function for k_s could be accomplished by the following computational means[2]: After obtaining the values of k_s to an accuracy of $\gtrsim$5 decimal points, $\xi_l(k_s)$ can be estimated from Eq. (8)

[2] The discussion in this subsection profited from a private communication with R. Samuelson (1972) of Goddard Space Flight Center.

for any given l. Then we may evaluate $W_s(\mu_i)$ for each discrete points from Eq. (10). Upon substituting $W_s(\mu_i)$ into Eq. (9), a new set of $\xi_\lambda(k_s)$ for any given λ can be further calculated. Usually $\xi_0(k_s)$, which was defined to be unity, is not equal to unity at this stage, while the $W_s(\mu_i)$ for all i generally blow up. We must then perform the computations of $\xi_\lambda(k_s)/\xi_0(k_s)$ so that $\xi_0(k_s)\equiv 1$ by definition. Presumably the $\xi_\lambda(k_s)$ become more accurate at this point so that by substituting them again into Eq. (10), an improved set of $W_s(\mu_i)$ should be obtained. We repeat the above procedures until the criteria

$$|W_s^{n}(\mu_i)-W_s^{n+1}(\mu_i)|<10^{-6}, \quad \text{for all } i,$$

are achieved, where the superscript n indicates the iteration steps. Thus, we obtain values of $W_s(\mu_i)$ accurate to $\gtrsim 5$ figures which are what we need in the intensity and flux computations.

d. Reduction of the order of simultaneous equations

After we obtain values of $\tilde{\omega}_l$, k_j, and the stabilized W-function, other quantities such as the H-, Z- and Planck's functions can be evaluated easily. We then solve the $2n$ simultaneous linear equations to derive the coefficients L_j by employing the boundary conditions described in the previous section. The following shortcuts are then applied so that the linear equations can be reduced to order n only. Consequently, by decreasing the order of the linear equations the computer time required will also be greatly reduced. To simplify the demonstrations, let the ground albedo $As=0$ for solar radiation, and assume that there are no contributions of radiation from the upper and lower Rayleigh layers for IR radiation. The latter case essentially applies to the window region (8–12 μm) where the atmosphere is primarily transparent. As a result of these simplifications, by substituting Eq. (14) into Eq. (16), and Eq. (24) into Eqs. (25) and (26) for determining L_j, we have

$$\sum_j L_j W_j(-\mu_i)=\begin{cases}-Z(-\mu_i), & \text{[SOL]}\\ -B_\nu(T), & \text{[IR]}\end{cases} \tag{31}$$

and

$$\sum_j L_j W_j(\mu_i)\exp(-k_j\tau_N)=\begin{cases}-Z(\mu_i)\exp(-\tau_N/\mu_0)\\ B_\nu(T_g)-B_\nu(T)\end{cases} \tag{32}$$

Adding and subtracting the above two equations, another set of simultaneous equations yield the forms

$$\sum_j L_j[W_j(-\mu_i)+W_j(\mu_i)\exp(-k_j\tau_N)]=\begin{cases}-[Z(-\mu_i)+Z(\mu_i)\exp(-\tau_N/\mu_0)]\\ B_\nu(T_g)-2B_\nu(T)\end{cases} \tag{33}$$

$$\sum_j L_j[W_j(-\mu_i)-W_j(\mu_i)\exp(-k_j\tau_N)]=\begin{cases}-[Z(-\mu_i)-Z(\mu_i)\exp(-\tau_N/\mu_0)]\\ B_\nu(T_g)\end{cases} \tag{34}$$

By noting the W-function symmetry relationships

$$\left.\begin{aligned}W_j(\mu_i)&=W_{-j}(-\mu_i)\\ W_{-j}(\mu_i)&=W_j(-\mu_i)\end{aligned}\right\}, \quad i,\, j(1,n), \tag{35}$$

we finally derive the following two sets of linear equations in which each set contains n equations and can be solved independently:

$$\sum_{j=1}^{n} M_j[W_j(-\mu_i)+W_j(\mu_i)\exp(-k_j\tau_N)]=\begin{cases}-[Z(-\mu_i)+Z(\mu_i)\exp(-\tau_N/\mu_0)]\\ B_\nu(T_g)-2B_\nu(T)\end{cases} \tag{36}$$

$$\sum_{j=1}^{n} N_j[W_j(-\mu_i)-W_j(\mu_i)\exp(-k_j\tau_N)]=\begin{cases}-[Z(-\mu_i)-Z(\mu_i)\exp(-\tau_N/\mu_0)]\\ B_\nu(T_g)\end{cases} \tag{37}$$

where

$$\left.\begin{aligned}M_j&=L_j+L_{-j}\exp(k_j\tau_N)\\ N_j&=L_j-L_{-j}\exp(k_j\tau_N)\end{aligned}\right\}. \tag{38}$$

Hence,

$$\left.\begin{aligned}L_j&=(M_j+N_j)/2\\ L_{-j}&=(M_j-N_j)\exp(-k_j\tau_N)/2\end{aligned}\right\}. \tag{39}$$

The above procedures for determining the coefficients $L_{\pm j}$ not only decrease the ranks of the matrix inversion calculations and substantially reduce computer time, but also serve the purpose of stabilizing the numerical computations for any given optical thickness τ_N, because Eq. (32) normally consists of very large and very small numbers in the form of $\exp(\pm k_j\tau_N)$.

While we may employ these processes for any cases of non-conservative scattering even for $\tilde{\omega}_0=0.99999$, unfortunately, they could not be extended to conservative scattering where $\tilde{\omega}_0\equiv 1$. The reason is because a new equation has to be re-derived for the upward and downward streams of radiation [see Eq. (15)], and consequently the symmetry relationships stated in Eq. (35) are no longer valid. It follows, therefore, that conservative scattering is the most difficult case to achieve higher accuracy in the numerical computations.

4. Comparisons with other methods

Since the discrete-ordinate method for radiative transfer has not been comprehensively explored and numerically verified, it seems to be extremely important to compare it with other established methods to obtain some quantitative justification. In recent years,

TABLE 1. Comparison of reflection and transmission (direct+diffuse) as computed by the discrete-ordinate method (DOM) with discrete-streams of 2, 4, 8 and 16 and by the doubling method for conservative and non-conservative scattering.

		Reflection μ_0			Transmission μ_0		
τ	Method	0.1	0.5	0.9	0.1	0.5	0.9
			a. $\tilde{\omega}_0=1$				
	DOM 2	0.41133	0.07635	−0.01294	0.58867	0.92365	1.01294
	4	0.40339	0.05743	0.03221	0.59661	0.94257	0.97593
0.25	8	0.40985	0.06937	0.02114	0.59015	0.93063	0.97888
	16	0.41768	0.07165	0.02246	0.58239	0.92842	0.97741
	Doubling	0.41610	0.07179	0.02250	0.58390	0.92821	0.97751
	DOM 2	0.51962	0.22559	0.02389	0.48222	0.77441	0.97611
	4	0.56631	0.22498	0.09826	0.43368	0.77501	0.90173
1	8	0.58967	0.24037	0.09582	0.41034	0.75963	0.90424
	16	0.58567	0.24068	0.09654	0.41440	0.75951	0.90249
	Doubling	0.58148	0.24048	0.09672	0.41852	0.75952	0.90328
	DOM 2	0.68564	0.49999	0.31612	0.31436	0.50001	0.68388
	4	0.73722	0.52120	0.34962	0.26278	0.47880	0.65036
4	8	0.73877	0.52046	0.34806	0.26124	0.47953	0.65203
	16	0.73541	0.51977	0.34776	0.26469	0.48053	0.65077
	Doubling	0.73254	0.51932	0.34823	0.26746	0.48069	0.65178
	DOM 2	0.86860	0.79100	0.71340	0.13140	0.20900	0.28660
	4	0.88407	0.78881	0.71005	0.11592	0.21118	0.28993
16	8	0.88397	0.78659	0.70755	0.11604	0.21260	0.29254
	16	0.88240	0.78702	0.70627	0.11770	0.21329	0.29225
	Doubling	0.88103	0.78659	0.70722	0.11897	0.21342	0.29279
			b. $\tilde{\omega}_0=0.80$				
	DOM 2	0.31802	0.05739	−0.01125	0.46566	0.84979	0.95403
	4	0.30269	0.04040	0.01746	0.46032	0.86090	0.92623
0.25	8	0.29599	0.04799	0.01473	0.44354	0.84949	0.92728
	16	0.29406	0.04888	0.01558	0.43120	0.84795	0.92679
	Doubling	0.28961	0.04855	0.01547	0.43017	0.84756	0.92669
	DOM 2	0.37519	0.14279	−0.00064	0.29023	0.55267	0.76333
	4	0.37646	0.12003	0.05425	0.22724	0.52936	0.72003
1	8	0.36938	0.12471	0.04901	0.20192	0.51471	0.71702
	16	0.36071	0.12396	0.04942	0.20416	0.51601	0.71784
	Doubling	0.35487	0.12342	0.04929	0.20556	0.51606	0.71772
	DOM 2	0.40411	0.20057	0.05152	0.06605	0.12281	0.20828
	4	0.39835	0.16792	0.09563	0.04412	0.10648	0.22130
4	8	0.38582	0.16755	0.08907	0.04453	0.10625	0.21918
	16	0.37725	0.16677	0.08944	0.04505	0.10710	0.21959
	Doubling	0.37148	0.16615	0.08925	0.04539	0.10718	0.21953
	DOM 2	0.40571	0.20354	0.05636	0.00018	0.00034	0.00060
	4	0.39914	0.16985	0.09945	0.00026	0.00063	0.00138
16	8	0.38661	0.16947	0.09280	0.00026	0.00062	0.00138
	16	0.37805	0.16870	0.09316	0.00027	0.00062	0.00139
	Doubling	0.37229	0.16808	0.09297	0.00027	0.00062	0.00139

significant progress has been made in analyzing the transfer of sunlight in planetary atmospheres including cloud and haze layers. One of the most powerful methods appears to be the "adding" method formulated some years ago by van de Hulst (1963). Since then, numerical computations and additional theory (including polarization) have been greatly developed, noticeably by Twomey *et al.* (1966), van de Hulst and Grossman (1968), Irvine (1968), Howell and Jacobowitz (1970), Hovenier (1971) and Hansen (1971a, b). Among these approaches, the concept of "doubling" is used so that the computations could be efficiently and accurately extended to homogeneous, optically thick scattering layers.

One of the goals of the theory of radiative transfer is its application in radiative balance studies in planetary atmospheres. The physical quantities which are necessary and sufficient for such studies are the vertical distributions of the fluxes. To demonstrate the usefulness of the discrete-ordinate method for radiation transfer in the flux evaluation for solar radiation, we have carried out the numerical computations for discrete-streams (i.e., the cosine of the emergent angles) of 2, 4, 8 and 16. From the results of these computations, we may obtain a quantitative comparison of how the simplified methods approach those of the more exact means. For example, we can compare the accuracies of the two- or four-stream approximations in flux com-

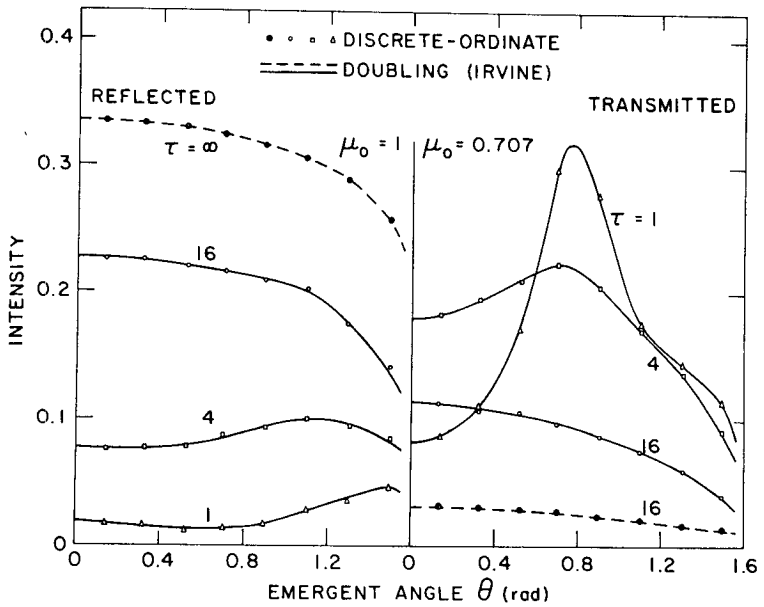

FIG. 3. Comparisons of the transmitted and reflected intensities obtained by the discrete-ordinate method with those reported by Irvine (1968) who used a combined Henyey-Greenstein phase function in doubling computations. The dotted lines are results for isotropic scattering.

putations, since the analytic solutions for the two simplified methods can be easily derived by means of the procedures outlined in the previous section. Thus, no complicated numerical experiments are needed, and the computer time required is almost negligible. In addition to these comparisons, K. Grossman (private communication) has kindly provided me with some of his numerical results based on the doubling method on which he worked with van de Hulst some years ago. With these additional data, the validity of the discrete-ordinate method appears to be more significant.

The comparison presented below required an accuracy up to five decimal points to justify quantitatively the discrete-ordinate method. These computations were all made for the analytic Henyey-Greenstein phase function

$$p(\Theta)=\frac{1-g^2}{(1+g^2-2g\cos\Theta)^{\frac{3}{2}}}, \tag{40}$$

with the asymmetry factor $g=0.75$. For the flux computations, the Henyey-Greenstein phase function is thought to be good enough to represent phase functions typical for clouds and hazes in the atmosphere. We have chosen the single-scattering albedo $\tilde{\omega}_0$ of 1 and 0.8 to cover the possible values in the visible and near IR of the solar spectrum for clouds and hopefully also for aerosols. The accuracy of the doubling method as described by van de Hulst and Grossman (1968) was about five figures.

Table 1 compares reflection and transmission (direct+diffuse) values obtained by using different discrete-streams of radiation and by the doubling method, for the cosine of solar zenith angles of 0.1, 0.5 and 0.9. The reflection r and the diffuse (t_{dif}) and direct (t_{dir}) transmission for solar radiation are defined as

$$\left.\begin{aligned} r&=F\uparrow(0)/\pi\mu_0F_0\\ t_{\text{dif}}&=F\downarrow(\tau_N)/\pi\mu_0F_0\\ t_{\text{dir}}&=\exp(-\tau_N/\mu_0)\end{aligned}\right\}. \tag{41}$$

The total transmission t is therefore equal to $t_{\text{dif}}+t_{\text{dir}}$. For discrete-streams of 16, the values of reflection and transmission are generally accurate up to ~3–4 digits for all three cases as compared with the doubling computations. The accuracy decreases to ~2 decimal points for discrete-streams of 8. It was found that reflection and transmission both have similar degrees of accuracy. For discrete-streams of 4, small deviations occur with the absolute differences in general on the order of ~0.01. This small amount of deviation from the more exact computations is certainly not at all significant for most optical thicknesses. Finally, the two-stream approximation appears to show fairly good accuracy for $\tau=4$ and 16 for both conservative and non-conservative scattering. However, the two-stream approximation tends to produce larger errors as the optical thickness decreases, especially for reflection because their values are generally small. At near-normal incidence, negative values are seen at $\tau=0.25$ for both cases. Hence, the two-stream approximation should be used with care. In general, we feel that the four-stream approximation may be good enough for studies of the

flux distribution in the transfer of solar irradiance through cloudy and turbid atmospheres.

Moreover, we have also carried out the comparisons by using two other asymmetry factors, 0.786 and 0.8, which represent sharper phase functions, Accuracy similar to that discussed above was found. In my previous investigation of the transfer of solar irradiance through cirrus cloud layers (Liou, 1973), I developed a simplified transfer method with an approximation made only in the integral form of the radiative transfer equation and showed an accuracy within 3% in most cases of conservative as well as non-conservative scattering. At that time, the comprehensive comparisons were made possible because J. E. Hansen (private communication) kindly provided me with some of his unpublished flux computations in which phase functions for clouds were used. I also made a comparison with his graphs and found that exact fitting of curves could be achieved by using discrete-streams of 8. Hence, the previous discussions should also apply reasonably well to clouds.

In addition to the flux, we have also made several comparisons for the azimuth-independent intensity computations with those obtained by other reliable methods. In the comparisons to follow, 16 Gaussian discrete streams were chosen for the discrete-ordinate method.

Fig. 3 compares the transmitted and reflected intensities with those published by Irvine (1968, Fig. 2) who also employed the doubling method for the purpose of rapid convergence in the numerical computations. The left- and right-hand sides of this figure are for the reflected intensity with the sun overhead ($\mu_0=1$) and for the transmitted intensity with $\mu_0=0.707$. These values are based on the assumption of a value of unity for the perpendicular flux to the stratification, i.e., $\pi\mu_0 F_0=1$. The solid lines are for anisotropic scattering in which two analytic Henyey-Greenstein phase functions were combined having an asymmetry factor of 0.786. Optical thicknesses of 1, 4 and 16 are displayed in the figure. The two dotted lines are the results for isotropic scattering. The comparison shows excellent agreement for all the cases presented as far as fitting by "eye" is concerned.

Fig. 4 shows a comparison of Rayleigh scattering with an optical thickness of 0.25. Since the values calculated by the exact solutions of Coulson *et al.* (1960) were for azimuth-dependent cases, we averaged their tabulated intensities (pp. 38–40, 312–314) over all azimuth angles so that a reasonable comparison could be made. Cosines of solar zenith angles μ_0 of 0.2, 0.6, 1.0 were selected. The solid curves were obtained from their tables with a surface albedo of zero. It should be noted that the incident flux F_0 in these tables is assumed to be unity. At $\mu_0=1$, because of the normal incidence, the reflected and transmitted intensities apply for all azimuth angles, and hence this case is essentially azimuth-independent. The comparisons reveal a fairly close agreement between the values obtained by the discrete-ordinate method and those of the exact solutions. The small discrepancies shown in this figure are understandable considering the important effects of polarization in the case of Rayleigh scattering [~5% errors produced by the scalar approximation

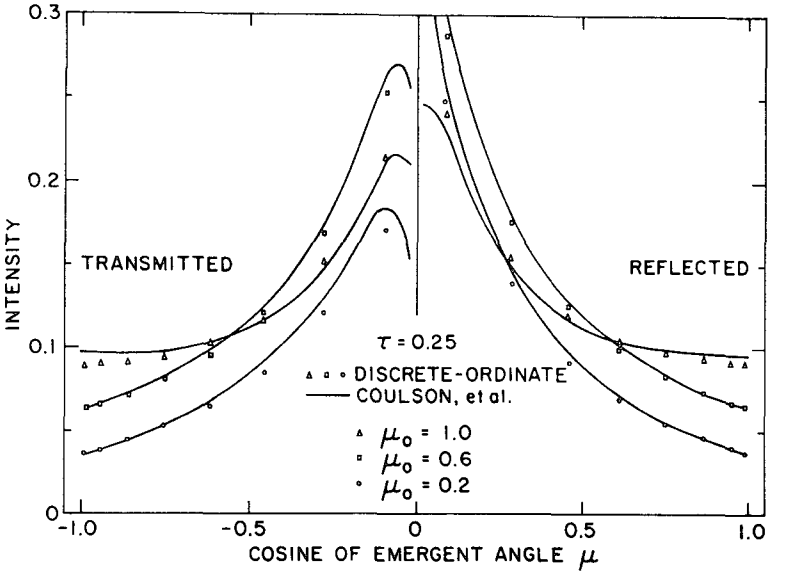

FIG. 4. Comparisons of the transmitted and reflected intensities for Rayleigh scattering calculated by the discrete-ordinate method with those by the exact solutions tabulated by Coulson *et al.* (1960). The values from the tables were averaged over azimuth angle. The optical thickness is 0.25 while the ground albedo equals zero.

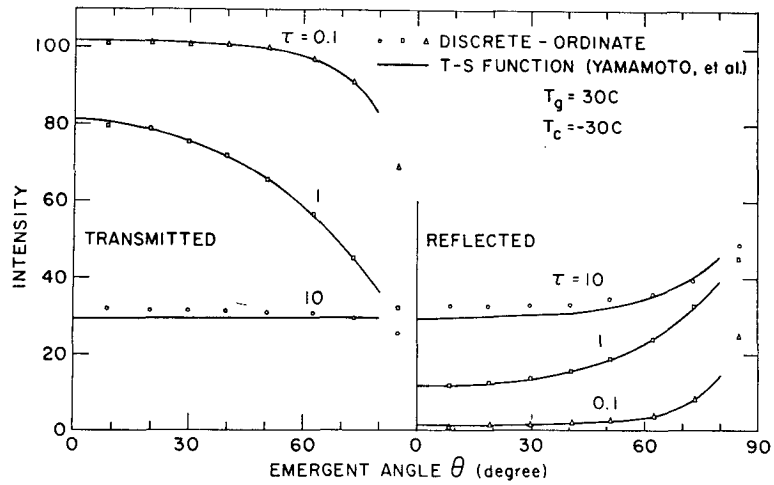

FIG. 5. Comparisons of the transmitted and reflected intensities from clouds at a wavelength of 10 μm evaluated by the discrete-ordinate method with those by the Chandrasekhar's S and T functions published by Yamamoto *et al.* (1966). The unit of intensity is 10^{-7} W cm^{-2} ster^{-1} (cm^{-1})$^{-1}$.

(Chandrasekhar, 1950)]. It is felt, however, that in the studies of the vertical flux distribution, the effects of polarization may possibly be eliminated.

So far we have compared the discrete-ordinate method for isotropic, Rayleigh, and anisotropic scattering with other established methods in the solar radiation region. We shall further carry out some quantitative comparisons in the thermal IR radiation region, although the transfer of IR radiation including the contributions of clouds or aerosols is seldom found in the published literature.

Fig. 5 illustrates a comparison with the results presented by Yamamoto *et al.* (1966; Figs. 4 and 6) who have investigated the transfer of IR radiation through water clouds in the 10-μm region. In their paper, computations were made by expanding the transmission and scattering functions (denoted as T and S) introduced by Chandrasekhar in a power series of the single-scattering albedo $\tilde{\omega}_0$. The Derimendjian's phase function which assumes real and imaginary parts of the refractive index of 1.212 and 0.0601, respectively, was used in their calculations. The ground and cloud temperatures are taken to be 30 and -30C, respectively. The numerical computations were said to extend to the second power of $\tilde{\omega}_0$ for $\tau=0.1$ and 1.0, and to the fourth power of $\tilde{\omega}_0$ for $\tau=10$. The comparison again reveals close agreement for $\tau=0.1$ and 1.0. It should be noted that their computations only extend to the emergent angle of 80°. For $\tau=10$, their values seem to be slightly underestimated. This is probably because more than four terms of $\tilde{\omega}_0$ expansions are needed for the larger τ. For thick clouds, the total intensity is primarily due to emission so that it becomes almost isotropic.

On the basis of the above comprehensive comparisons, we therefore conclude that the discrete-ordinate method for radiative transfer either in the solar or IR radiation regions is a useful and reliable method. Hence, we wish to point out some potential applications of this method for radiation studies in turbid and cloudy atmospheres.

5. Some applications to cloudy and hazy atmospheres

In the previous sections, following the theoretical and numerical analyses, we have further verified quantitatively the high accuracy of the values of the transmitted and reflected intensities and fluxes obtained by the discrete-ordinate method by comparison with other established methods, particularly those involving doubling procedures. The discrete-ordinate method employs a completely different approach in solving the multiple-scattered radiation field, i.e., the analytic solutions of the intensity distribution can be derived with the unknown coefficients determined numerically by the given boundary conditions in the atmosphere. While the radiation field on the boundaries, which most of the radiative transfer methods are generally concerned with, can be computed, the internal radiation field can also be evaluated very easily without any additional computational efforts. In this section, we shall demonstrate the usefulness and the applicability of the discrete-ordinate method in the studies of the distributions of intensity, flux, and the heating and cooling rates in the atmosphere. Applications will be given at monocromatic wavelengths, 0.7 and 1.5 μm representing the visible and near-IR solar radiation and 10 μm the thermal IR radiation. No attempt is made to include the complete solar and IR spectrum in this study.

TABLE 2. Optical properties for clouds and hazes.

λ	Cloud (gamma function, $r_m=4$ μm)				Haze (power law, $\nu^*=3$)			
(μm)	n_r	n_i	$\tilde{\omega}_0$	$\langle\cos\Theta\rangle$	n_r	n_i	$\tilde{\omega}_0$	$\langle\cos\Theta\rangle$
0.7	1.33	0.0	1.0	0.84802	1.54	0.001	0.98787	0.62082
1.5	1.318	0.0002065	0.99025	0.82662	1.54	0.01	0.89823	0.62653
1.0	1.214	0.05316	0.63828	0.86473	1.80	0.1	0.51592	0.52249

a. Single scattering

The distribution of scattered energy due to single scattering from a polydisperse system of particulates may be described by the phase function, which is determined primarily by the size distributions as well as the optical properties of the particulates in the atmosphere. We have used the theoretical functions of

$$\frac{dn(r)}{dr}=\begin{cases} cr^6\exp(-6r/r_m) \\ c'\exp[-(\nu^*+1)] \end{cases} \tag{42}$$

for water clouds and hazes, respectively. The first is the modified gamma function suggested and used previously by Deirmendjian (1969) for clouds, while the second represents the well-known power law distribution for aerosols (Junge, 1963). In Eq. (42), $dn(r)$ denotes the number density of particles with radii between r and $r+dr$, and c and c' are constants to be determined from the total number density of clouds and hazes, respectively. Furthermore, a mode radius r_m of 4 μm and an index ν^* of 3 were employed in this study. Although the observed cloud drop-size distributions are often remarkedly different from the modified gamma functions, especially in the tail regions of the large particles, they do represent some drop-size distributions for fair weather cumulus (Liou and Schotland, 1971). With respect to the size distributions for aerosols, the value of ν^* is generally assumed to lie between 2.5 and 4. Hence, the selection of $\nu^*=3$ hopefully should also represent certain aerosol-size distributions in the atmosphere.

The real and imaginary parts of the refractive index for water drops were taken from Irvine and Pollack (1968), while for aerosols we used the recent values reported by Volz (1971) for water soluble aerosol substance. These values are all given in Table 2 along with the single-scattering albedo $\tilde{\omega}_0$ and the asymmetry factor $\langle\cos\Theta\rangle$. The uncertainties of the imaginary parts of aerosols in the visible and near IR are expected. However, the extremely difficult problems of the absorption properties of atmospheric aerosols are beyond the scope of this study.

Mie scattering computations for polydisperse water drops and aerosols (Liou and Hansen, 1971) were carried out by using the drop-size distributions described in Eq. (42). Gaussian integration for the particle size was employed in which the integrations were performed to the upper limits of 14 μm and 5 μm for clouds and hazes, respectively. Fig. 6 shows the phase functions of clouds and hazes. For clouds illuminated by a visible

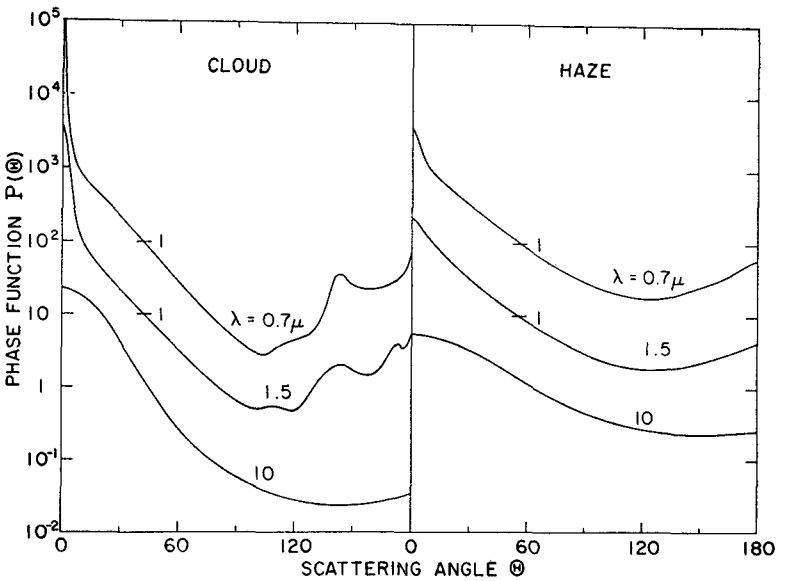

FIG. 6. Phase functions of cloud and haze for incident wavelengths of 0.7, 1.5 and 10 μm. The vertical scale applies to the lowest curves, while the upper curves are displaced upward by a factor of 10.

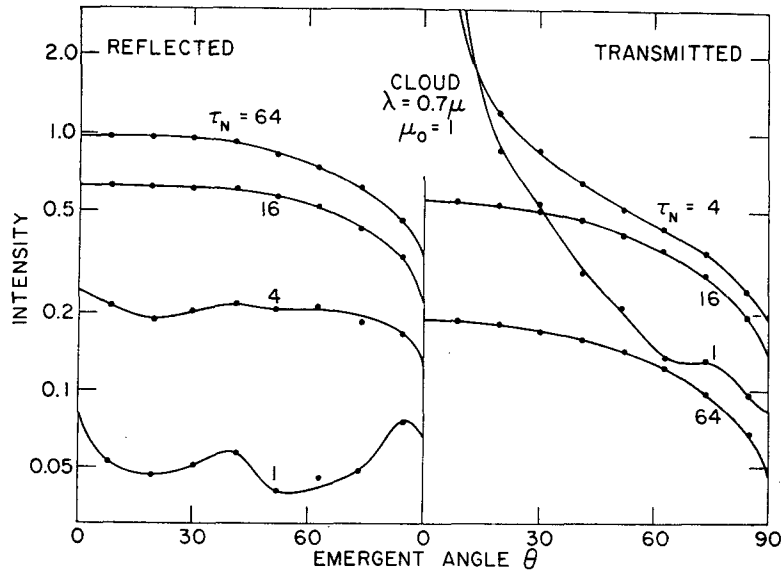

FIG. 7. The transmitted and reflected intensities as a function of the emergent angle (with respect to the zenith) for clouds illuminated by a wavelength of 0.7 μm at normal incidence. The solid lines are connected by the eye.

wavelength of 0.7 μm, the feature shown at a scattering angle of $\sim$140° is the well-known primary cloudbow which arises from rays internally reflected once in the drops. This cloudbow reduces its strength at $\lambda=1.5\,\mu$m because of small absorption and smaller size parameter ($2\pi r/\lambda$). The glory generated by surface waves which occurs at $\sim$180° for $\lambda=0.7\,\mu$m seems to move toward the smaller scattering angle for $\lambda=1.5\,\mu$m. Two important points should be noted for hazes.[3] First, the Fraunhofer diffraction peaks as shown earlier for cloud drops are much less pronounced. In addition, it is also interesting to note that the values of the back peaks for aerosols appear to have similar orders of magnitude as those of cloud drops when the refractive indices given in Table 2 are used. Recent investigations of the backscattering from atmospheric aerosols seem to indicate that owing to their non-spherical properties, the amount of backscattered intensities are reduced substantially (Holland and Gagne, 1970; Waggoner *et al.*, 1972). Finally, at $\lambda=10\,\mu$m, due to the large absorption involved, neither cloud drops nor aerosols produce significant scattering features.

On the basis of the single-scattering properties discussed above, the following radiation computations may therefore be carried out.

b. Intensity and flux distribution

1) SOLAR RADIATION

The intensity distributions on the boundaries of cloudy and hazy layers are shown in Figs. 7 and 8 for various optical depths illuminated by solar radiation. In all cases to be presented, the albedo of the ground (As) is assumed to be zero. The reflected and transmitted intensities as functions of the emergent angle (with respect to the zenith) for clouds at $\lambda=0.7\,\mu$m are given in Fig. 7 for normal incidence ($\mu_0=1$) assuming that the solar incident flux $F_0=1$. All directions of scattering can be shown for the case where the sun is at normal incidence. In this figure the black dots denote values of the intensity at each discrete-stream. These values are connected and extrapolated by eye. The reflected intensity shows limb-darkening for optical depths of 16 and 64. For optical depths of 1 and 4, however, the finite discrete points do not describe closely the fluctuating characteristics of the intensity distributions. Such fluctuations are caused by the strong forward-scattering nature of the phase function of clouds. The diffusely transmitted intensity, on the other hand, decreases sharply with increasing emergent angles for these two cases. Similar patterns are illustrated for hazes incident by a visible wavelength of 0.7 μm (Fig. 8), but with much smaller optical thicknesses (0.125, 0.25, 0.5 and 1). Figs. 9 and 10 show the results of reflection and transmission for clouds at $\lambda=0.7$ and 1.5 μm. We interchange the reflection and albedo (local) terms in the following discussions. At $\lambda=0.7$ μm (Fig. 9), the albedo of clouds increases rapidly with increasing optical thickness, because no absorption takes place within the cloud layers. A typical cloud having an optical thickness of $\sim$20 would have an albedo of $\sim$70% up to the zenith angles of 60°. For $\tau=1$, the transmission pattern has a peak at a zenith angle of $\sim$60° without counting the direct transmitted component. At $\lambda=1.5$ μm, cloud particles absorb a small portion of energy (see Table 2). Hence,

[3] Recently, Braslau and Dave (1973) also made computations for the transfer of solar radiation through hazy atmospheres.

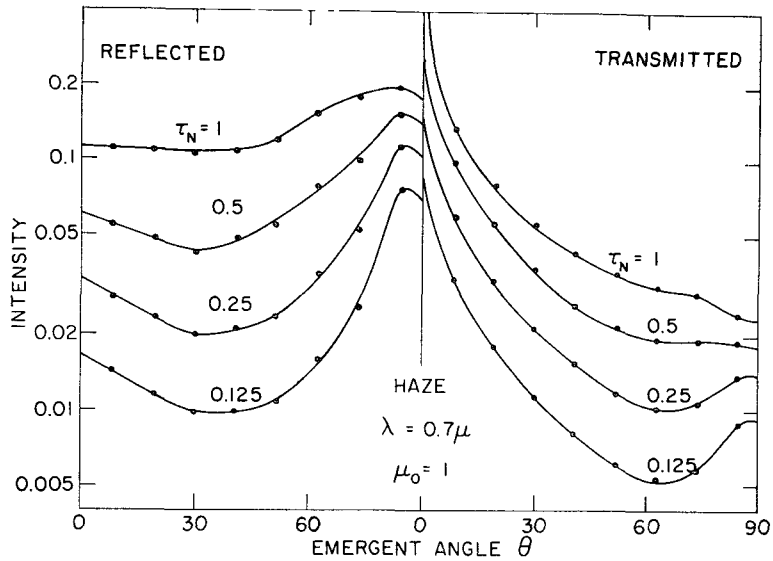

FIG. 8. Same as Fig. 7 except for haze.

the diffuse reflection and transmission for $\tau=1$ and 4 have distributions similar to those for $\lambda=0.7$ μm. However, such a small amount of absorption effectively reduces both the values of reflection and transmission for large optical thickness. The variations of the optical thickness of clouds due to the wavelength can be neglected in the visible and near-IR region, because the cloud particles at these wavelengths approach the geometrical optics region. Consequently, the associated extinction coefficients may be considered as about the same. Thus, from these computations we found that the decrease of the albedo for a typical cloud layer ($\tau\approx20$) caused by a small portion of absorption is on the order of 20%. A similar reduction is also shown in the values of transmission. For the case of $\tau=64$, it is seen that no flux transmits through the cloud layers. Fig. 11 illustrates the diffuse reflection and transmission for hazes illuminated by a wavelength of 0.7 μm. The albedo of hazes increase sharply with increasing zenith angles.

In order to obtain some quantitative information on the absorbed solar energy within clouds and hazes, we calculated the absolute values of the monocromatic absorption from

$$a_\lambda=\mu_0 f_\lambda(1-r_\lambda-t_\lambda), \tag{43}$$

where f_λ [$=\pi F_0$] denotes the monochromatic solar flux outside the atmosphere per unit area. From the *Handbook of Geophysics* (1960), f_λ at $\lambda=0.7$ and 1.5 μm were estimated to be about 0.1499 and 0.02517 W cm^{-2} μm^{-1},

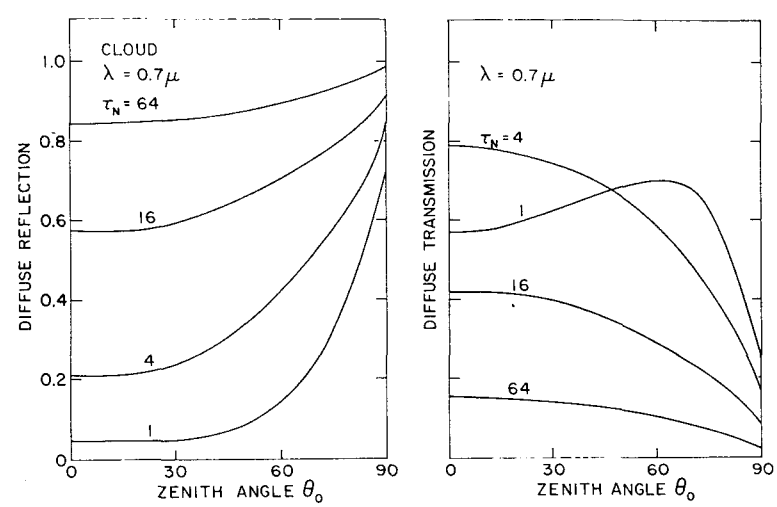

FIG. 9. The diffuse transmission and reflection (albedo) as a function of the solar zenith angle for several optical thicknesses of clouds illuminated by a wavelength of 0.7 μm.

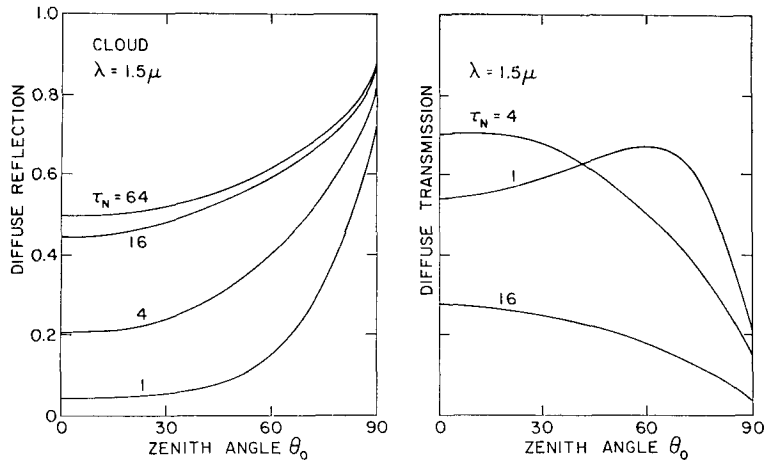

FIG. 10. Same as Fig. 9 except for a wavelength of 1.5 μm.

respectively. With these values, we can present the monochromatic absorption of solar irradiance as functions of the solar zenith angle. These are demonstrated in the right-hand (clouds) and left-hand (hazes) sides of Fig. 12. The single-scattering albedo at $\lambda = 1.5$ μm for cloud particles is about 0.99, indicating that absorption due to cloud particles experienced from a single scattering would be expected to be negligible. However, after photons have been multiply-scattered a number of times, appreciable amounts of absorption occur for thick clouds as seen in this figure. The values of absorption decrease with increasing zenith angles when the dependence of the solar energy on its position is taken into consideration. For $\tau = 64$, approximately 45% of the solar irradiance is absorbed within the cloud deck for zenith angles up to ~40°, while the absorption only reduces to ~25% for an optical thickness of four times less ($\tau = 16$). The above calculations then crucially indicate that the absorption of solar irradiance in the near-IR spectrum cannot be ignored, since at least 30% of the entire solar energy lies in this region. Unfortunately, accurate imaginary portions of the refractive indices for ice and water are not available at wavelengths from 0.7 to 1.0 μm, and they are generally considered to be zero. As for hazes, although the monochromatic incident flux at a wavelength of 0.7 μm is about six times larger than that at 1.5 μm, the absolute absorption is smaller for all four optical thicknesses because a factor of 10 difference in the imaginary parts of the refractive indices is used. Finally, we shall point out that the correct way to investigate the absorption within clouds and hazes would be to integrate the monochromatic absorption of solar irradiance over the entire solar spectrum.

2) THERMAL IR RADIATION

Computations of the transfer of thermal IR radiation through clouds and hazes have been made for several

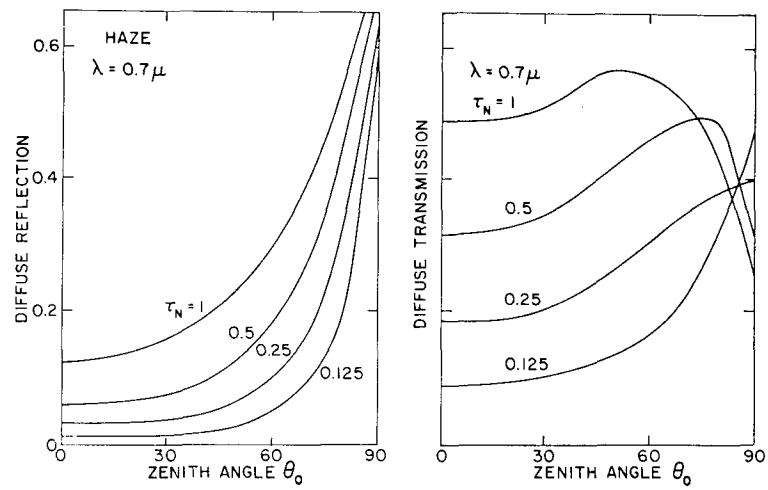

FIG. 11. The diffuse transmission and reflection as a function of the solar zenith angle for various optical thicknesses of haze illuminated by a wavelength of 0.7 μm.

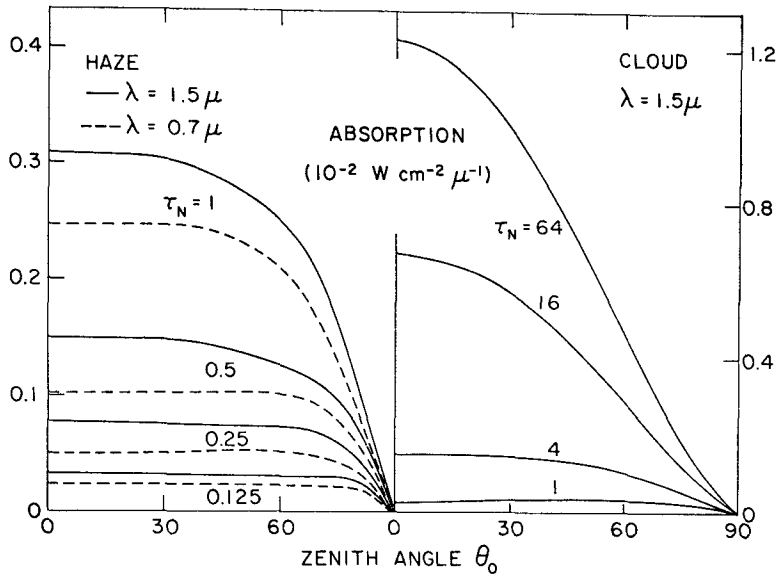

FIG. 12. The amount of monochromatic absorption within cloud and haze layers as a function of the zenith angle for a number of optical thicknesses. Two different scales for the cloud and haze are shown.

atmospheric models employing a monochromatic wavelength of 10 μm for which atmospheric effects below and above the scattering and emitting layers are negligible. These models consist of various values of the optical thickness and the isothermal temperature of the cloudy and hazy layers, as well as the temperature of the ground which emits the IR radiation isotropically.

Figs. 13 (for clouds) and 14 (for hazes) illustrate the relative transmitted and reflected intensities as functions of the emergent angle in units of $\pi B_\nu(T_g)$, assuming a ground temperature of 15C. Again, discrete-streams of 16 were used in the computations, and the continuous curves were obtained by connecting the discrete points and extrapolating to 0° and 90°. For clouds, the extinction coefficient at $\lambda = 10\,\mu$m is about half of those at the visible and near-IR wavelengths, and we have therefore employed optical thicknesses of 1 and 10 in the numerical calculations. It should be noted that the intensity distributions for $\tau \geqslant 10$ are practically the same as those at $\tau = 10$. Three cloud temperatures, 10, 0 and −10C, are shown in this figure. The transmitted as well as the reflected intensities from thin clouds depend slightly on the cloud temperature because the emission from the ground dominates the

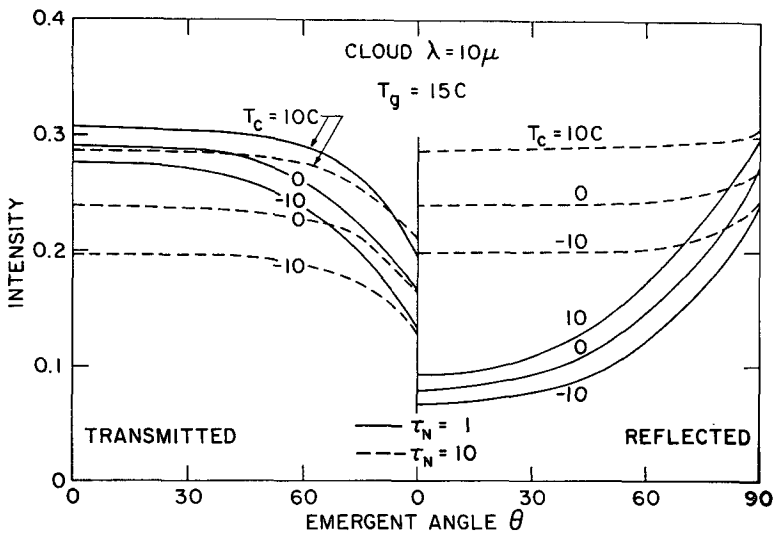

FIG. 13. The transmitted and reflected intensities from clouds at a wavelength of 10 μm. The ground temperature is assumed to be 15C. Several cloud temperatures and optical thicknesses are illustrated. The vertical scale is in units of $\pi B_\nu(T_g)$.

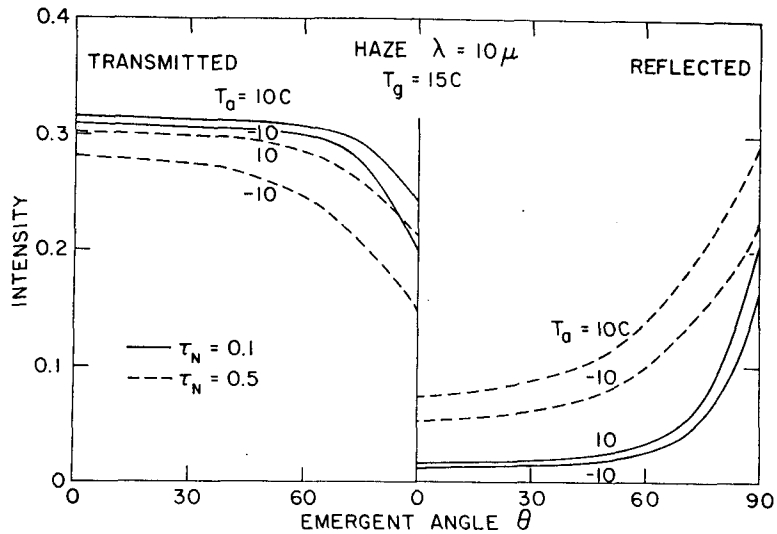

FIG. 14. Same as Fig. 13 except for haze.

radiation process. The transmitted intensity shows a limb-darkening, while the reflected intensity indicates a strong limb-brightening. In cases of thick clouds, the transmitted and reflected intensities are due primarily to the emission of the cloud layers so that the intensity patterns become almost isotropic, as shown especially in the reflected intensity patterns. Moreover, the values of the transmitted intensity for $\tau=1$ and 10 appears to have smaller differences which demonstrate that thick clouds may function as the underlying surface. The intensity distributions for hazes are shown in Fig. 14 where optical thicknesses of 0.1 and 0.5 are chosen because the extinction coefficient at $\lambda=10\,\mu$m is about 10 times smaller than that at visible wavelengths. Since hazes are optically thin with respect to thermal IR radiation, the transmitted intensity depends strongly upon the ground temperature. The thin hazes apparently destroy the isotropic radiation pattern emitted from the ground. The values of the reflected intensity are found to be rather small, but they increase drastically toward the limb.

The reflection r and the transmission t of the thermal IR radiation for clouds and hazes are defined accordingly as

$$\left.\begin{aligned} t&=F\uparrow(0)/[\pi B_\nu(T_g)] \\ r&=F\downarrow(\tau_N)/[\pi B_\nu(T_g)] \end{aligned}\right\}. \tag{44}$$

On the basis of the above definition, the values of transmission represent essentially the effects of clouds or hazes on the outgoing flux $[=\pi B_\nu(T_g)]$. If the ratio becomes unity, then the interferences of clouds or hazes

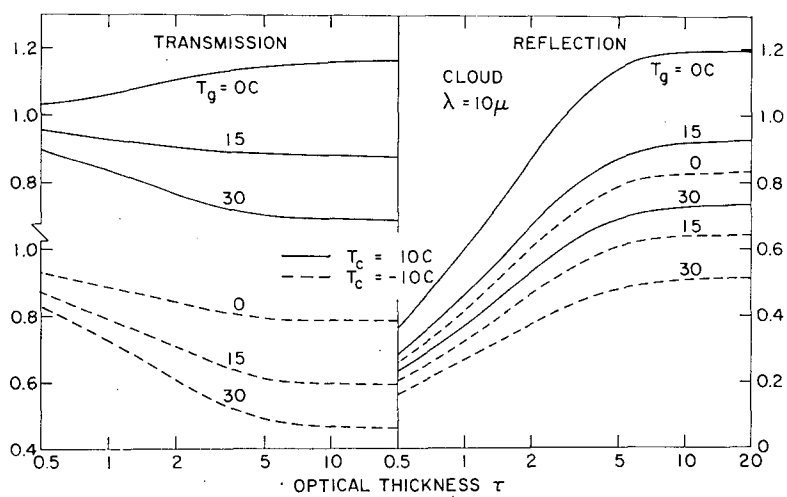

FIG. 15. Transmission and reflection of IR radiation (see text for definition) as a function of the optical thickness for various cases of cloud and ground temperatures.

may be entirely neglected. Fig. 15 shows the transmission (left-hand side) and reflection (right-hand side) as functions of the optical thickness for several combinations of cloud and ground temperatures. The transmission decreases with increasing optical thickness except when a warm cloud occurs above cold ground. For $\tau>10$ (with respect to $\lambda=10\,\mu$m), a cloud with a temperature of -10C would reduce the outgoing flux emitted from a typical ground temperature of 15C by $\sim 40\%$. For the same ground temperature, a warm cloud at 10C would only reduce the outgoing flux by $\sim 10\%$ because the emission from the cloud itself becomes predominant. Increasing the ground temperature results in decreasing the transmission, and hence the effects of clouds on the outgoing radiation become more important. On the other hand, the values of reflection become significant only when the cloud thickness becomes large. Thick clouds may be thought of as trapping the outgoing radiation from below and consequently keeping the atmosphere under them warm. Fig. 16 illustrates the corresponding results of transmission and reflection computations for hazes. While the values of transmission are close to unity for $\tau<0.2$, the reflection is almost negligible.

Although only one monochromatic wavelength ($10\,\mu$m) was employed in the above computations, the physical arguments may be applied reasonably well to the entire window region (~ 8 to $\sim 12\,\mu$m) where the size parameters and the refractive indices for water and ice particles vary slightly.

c. *Net flux and heating and cooling rates*

The net flux at any given level τ can be written as

$$F_N(\tau)=F\uparrow(\tau)+F\downarrow(\tau), \tag{45}$$

where the total downward flux in our notation is denoted

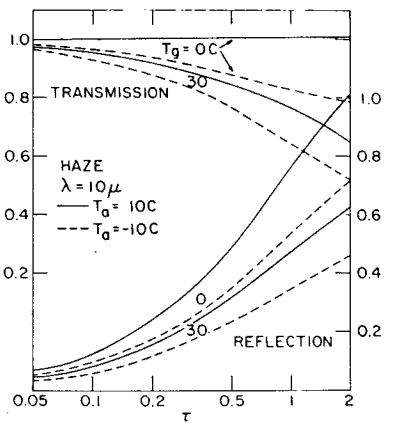

FIG. 16. Same as Fig. 15 except for haze.

as negative. For conservative scattering, the same net flux is obtained throughout the scattering layer, since absorption of radiation does not take place. If the particulates absorb and/or emit radiant energy, the differential differences of net fluxes in an infinitesimal layer will then produce the warming or cooling for this layer from the principle of conservation of energy. Thus, the heating or cooling rate experienced by a layer of air due to the effect of radiation transfer may be expressed in height coordinates as

$$\left(\frac{\partial T}{\partial Z}\right)_R \approx -\frac{1}{\rho c_p}\frac{\partial F_N}{\partial Z} \approx -\frac{1}{\rho c_p}\frac{F_N(Z+\Delta Z)-F_N(Z)}{\Delta Z}, \tag{46}$$

where ρ is the air density and c_p the specific heat at constant pressure. In addition to the absorption due to particles, water vapor also absorbs thermal IR as well as solar irradiance. The influence of water vapor in determining heating and cooling rates within the scat-

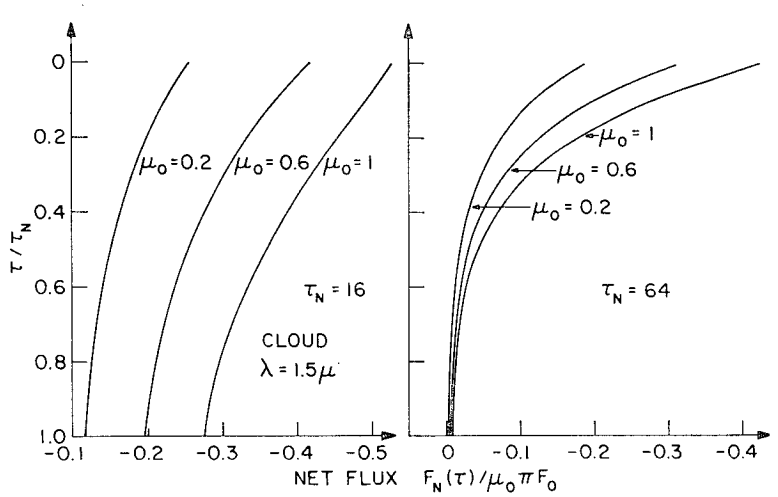

FIG. 17. The net flux for the transfer of 1.5-μm solar irradiance through cloud layers. The vertical and horizontal scales are normalized dimensionless parameters.

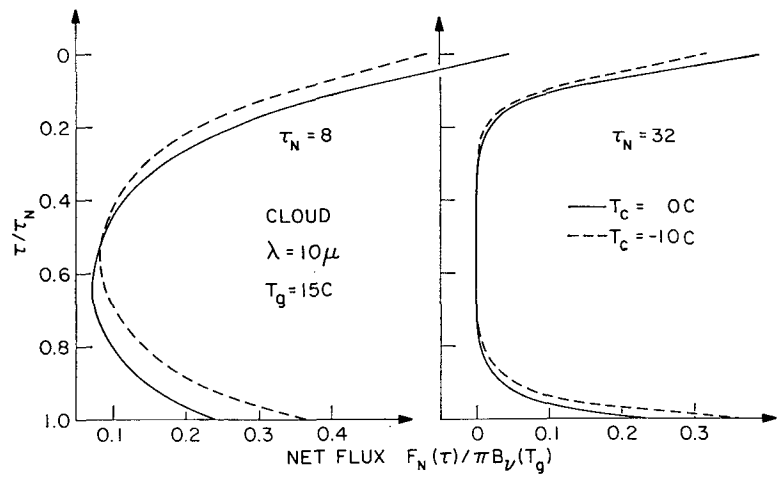

FIG. 18. The net flux for the transfer of 10-μm thermal radiation through cloud layers.

tering layer is of vital importance, and we would like to include its contribution in future investigations. It is assumed that the monochromatic volume extinction cross sections of the particulates are constant throughout the cloudy or hazy layer so that the optical thickness and the height can be interchanged without any complication. Furthermore, in the computations which follow, vertical resolutions of 20 points are used.

Fig. 17 shows the net flux of the transfer of 1.5-μm solar irradiance within cloud layers having optical thicknesses of 16 and 64. In this figure, the vertical scale is a normalized dimensionless parameter which is zero at the cloud top and one at the bottom, while the horizontal scale represents the value of net flux assuming unity incident solar flux perpendicular to the plane-parallel stratification. The negative net flux indicates that the downward radiation component is greater than the upward component so that solar heating takes place within the layer. The cosines of zenith angles of 0.2, 0.6 and 1 were adopted in the computations to investigate the variation of net flux caused by the changing of the sun's position. For a cloud having a very large optical thickness of 64, negligible net flux is found in the lower portion of the layer due to the large extinction of cloud particles. A large gradient of net flux is seen near the cloud top. As a result, one would expect that solar heating within an optically thick cloud occurs mostly near the upper portion of the cloud layer. The net flux decreases with increasing solar zenith angle because the direct downward flux is reduced according to $\exp(-\tau/\mu_0)$. For a typical cloud whose optical thickness is 16, the reduction of net flux with cloud depth is not as large as compared with the previous case. A decrease in the net flux for greater zenith angles is clearly evident in this figure.

Fig. 18 shows the net flux for the transfer of 10-μm irradiance through cloud layers which have optical thicknesses of 8 and 32. In the IR wavelengths the radiation sources arise primarily from the ground as well as the cloud particles from which radiation interacts in a complicated manner involving absorption, emission and multiple scattering. We have normalized the thermal-IR net flux with respect to the flux emitted from the ground which is assumed to have a temperature of 15C. For $\tau_N=8$, a cloud with a temperature of 0C shows large values of positive net flux at the upper portion. It decreases with increasing thickness and has a minimum at a level of $\tau\approx 5$ (slope turning point), then increases all the way to the cloud base. A colder cloud of -10C reduces the net flux at the cloud top but increases the values of net flux near the lower portion of the layer. For a very thick ($\tau_N=32$) cloud, near-zero values of net flux are observed within most of the center portion of the layer, whereas significant amounts of net flux are obtained at both the cloud top and base.

From these illustrations we obtain an IR radiation picture as follows: clouds emit radiation in all directions, while they receive additional radiation from the ground. The increase of the upward radiation with the height in the upper parts of the cloud arises from the accummulation of emission and scattering from below, since we assume that no downward radiation reaches the cloud top. On the other hand, the lower portion of the cloud receives the radiation emitted from the ground so that the largest value of the upward flux is found at the cloud base. Moreover, the cloud temperature (assumed to be isothermal) has some effect on the net flux distribution. Generally speaking, typical clouds would undergo warming near the base and cooling at the top. We shall explain this important consequence in the next figure.

Cloud particles absorb solar radiation at visible and near-IR wavelengths. For typical clouds, such absorption may be built up significantly as we noted earlier. This amount of absorption will then be used to heat the cloud layer. Meanwhile, ground and clouds emit

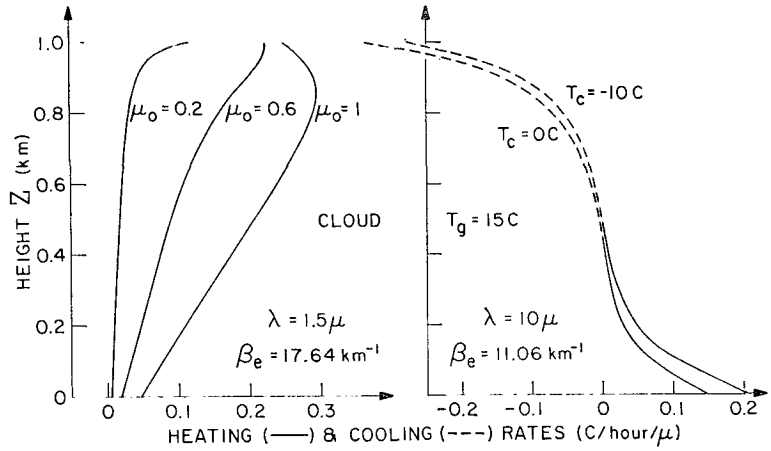

FIG. 19. The heating and cooling rates as functions of the height within a cloud 1 km in thickness. The volume extinction coefficients of cloud particles at wavelengths of 1.5 and 10 μm are indicated.

longwave radiation having maximum energy centered at about 8–12 μm in normal conditions. Since such radiation is either absorbed or scattered by the cloud particles, both heating and cooling mechanisms are possible within the layer during transfer processes. The right-hand side of Fig. 19 demonstrates the solar heating and the left-hand side the IR heating as well as cooling, assuming a cloud thickness of 1 km. The volume extinction coefficients for water droplets at 1.5 and 10 μm are 17.64 and 11.06 km^{-1}, respectively, based on Mie calculations for the size-distribution described previously. The heating and cooling rates are given in units of degrees per hour per wavelength. For solar radiation, the heating rate depends vitally upon the solar zenith angles. At a normal incidence, the maximum heating rate is found not at the top but about 100 m below it. Heating rates decrease toward the cloud bottom as expected. Decreasing the solar zenith angle results in decreasing the heating rate. For near-grazing incidence, heating occurs only at the cloud top because photons suffer longer paths. As for thermal IR radiation, we found in this particular case that the cloud top undergoes strong cooling while heating takes place near the base. The temperature dependence appears to be important; for 10C differences in cloud temperature, a 0.1C hr^{-1} μm^{-1} heating or cooling rate may result at the cloud bottom or top. At night when the solar heating can be ignored, the combinations of base warming and top cooling within the cloud cause the lapse rate to become steeper, hastening cloud destabilization. If we assume that the cloud particles possess the same properties in the window region, and take an isothermal temperature of -10C, the cloud top cooling would result in a lapse rate of $\sim$1C hr^{-1} between the top and a level about 100 m below the top. At the same time the cloud base warming would experience a lapse rate of $\sim$0.5C hr^{-1} between the base and a level about 100 m above the base. This fact perhaps provides explanations of why stratiform clouds frequently tend to develop into cumuliform in the evening. Convective and turbulent mixing, however, could prevent such destabilization of stratified clouds. During the daytime strong solar heating at the upper portions of the cloud may lead to the equilibrium state so that base-warming and top-cooling phenomena may not be easily developed. Although the solar and IR radiative heat transfer within a cloud interact in a rather sophisticated manner, we have demonstrated that a reliable model can be established to describe completely the radiative heat balance of the cloud on a time scale of the order of an hour to a day.

Fig. 20 shows the heating and cooling rates within a hypothetical haze. Since a number of uncertainties such as the number density, the absorption coefficients, and the vertical inhomogeneity associated with the optical properties of aerosols, are involved, use was made of the dimensionless vertical scale with optical thicknesses

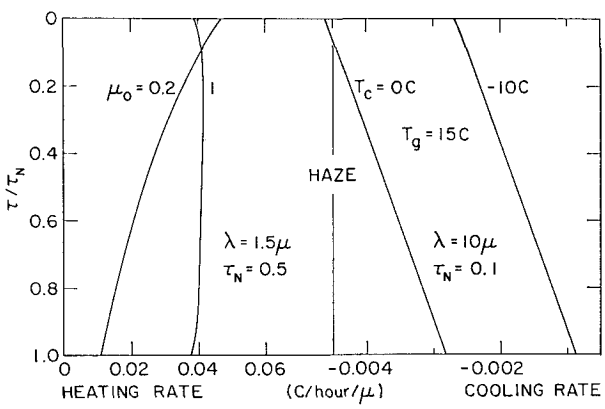

FIG. 20. The heating and cooling rates for a hypothetical haze having optical thicknesses of 0.5 and 0.1 at wavelengths of 1.5 and 10 μm, respectively. The vertical scale is a normalized dimensionless parameter.

of 0.5 and 0.1 for haze at wavelengths of 1.5 and 10 μm. It should be noted again that the optical thickness of aerosols varies strongly with wavelength. The heating rate for normal incidence is more or less constant, decreasing slightly with increasing solar zenith angle. In addition, we also note that the heating rate at the top for near-grazing incidence is greater than that for normal incidence. The IR cooling rate decreases with thickness almost linearly. The dependence of haze temperature on the cooling rate is easily seen in this figure.

All the above computations were carried out by employing discrete-streams of 16 in the discrete-ordinate method. We shall now discuss briefly the accuracy of using the simpler discrete-streams of 2 or 4 in the evaluation of heating and cooling rates. Since these rates are estimated by the finite differences of the net flux, errors produced in the flux computations accumulate or cancel. Studies made for the cases presented in Fig. 19 for clouds reveal the following approximate values: for solar radiation, the method of discrete-streams of 4 introduces absolute errors (the differences between the values computed by the method of discrete-streams of 4 and those by means of discrete-streams of 16) of <0.03C hr^{-1} μm^{-1}, while for longwave radiation the errors are <0.01C hr^{-1} μm^{-1}. Errors resulting from using discrete-streams of 2 are about two to three times larger. As for thin haze, because of several uncertain factors involved in the computations of heating and cooling rates, we shall not make any indication at this point.

6. Conclusion

We have developed a radiative transfer method by replacing the integral in the transfer equation by a discrete Gaussian quadrature. As a result of such a substitution, a set of first-order, nonhomogeneous differential equations can be derived, from which the explicit solutions and corresponding eigenvalues may subsequently be obtained. It is shown that the explicit solutions for solar and IR radiation yield similar forms in which the source function for the former consists of the direct radiation component from the sun and that for the latter the emission from the particulate layers. Numerical procedures are required only to determine the proportional coefficients from the boundary conditions of the radiation field in the atmosphere.

For the convenience of discussion and presentation and for studies of the accuracy of the method, we have chosen discrete-streams of 2, 4, 8 and 16 in the numerical computations. Comparisons with other transfer techniques for results of isotropic, Rayleigh and anisotropic scattering indicate that the use of discrete-streams of 16 yields close agreement. It is also pointed out that solutions employing discrete-streams of 2 and 4 can be expressed without complicated numerical means. The computer time involved for the case of 16 normally takes less than 2 min on the CDC 6400 computer (without counting the computer time for the Mie calculations), while for the rest of the three cases, no more than 20 sec are needed.

Radiation transfer computations using other techniques are generally carried out by means of successive iterations, which take considerable amounts of computer time in order to extend the calculations to optically thick layers. The numerical procedures based on the discrete-ordinate method, however, do not depend upon the optical thickness since the solutions of the radiation field are explicitly derived. In addition to the relatively economic way of solving radiation transfer through particulate atmospheres, the present method also provides an easier means for the evaluation of the net flux, and hence of the heating and cooling rates within particulate layers. It remains to be demonstrated that similar computational procedures can be used to include azimuth-dependent terms and to extend the theory to the case of polarization for the scattering of sunlight.

With regard to various radiation calculations for meteorological applications, in addition to the problems of composition, thickness and size-distribution of the particulate layer, one has to take the wavelength dependency of the radiation into account along with the optical properties of the particulates. Furthermore, if time or space scales should also play a role in the radiation computations, the resulting increase in the amount of computer time required would be so tremendous that some sort of parameterization would have to be performed. The discrete-ordinate method that we have developed seems to provide such an approach. We have made a number of applications by utilizing monochromatic wavelengths. These applications, involving both solar and thermal IR radiation, consist of computations of the reflected and transmitted intensity and flux for clouds and hazes, as well as the net flux and the heating and cooling rates within them. From these illustrations, it appears that the method can be extended without great difficulty to the entire solar and IR spectrum so that a realistic radiative balance model for cloudy and hazy atmospheres could be established. It may be that the method can be used as a first attempt to incorporate a reliable radiation treatment into general circulation models.

Acknowledgments. The author wishes to thank Profs. R. G. Fleagle and C. B. Leovy and Drs. R. Samuelson and J. E. Hansen for reading the manuscript and offering suggestions. This research was supported by the National Science Foundation under Grant GU-2655.

APPENDIX

Matrix Method for the Eigenvalue Problem

The basic associated homogeneous differential equations for the discrete-ordinate method in the nth

approximation can be written as

$$\mu_i \frac{dI(\tau,\mu_i)}{d\tau} = I(\tau,\mu_i) - \tfrac{1}{2}\sum_{l=0}^{N} \tilde{\omega}_l P_l(\mu_i) \sum_j a_j P_l(\mu_j) I(\tau,\mu_j), \tag{A1}$$

where we let $i, j = 1, 2, \ldots, n$ to avoid the confusion of the subscripts in the following development. We define

$$C_{ij} = \tfrac{1}{2}\sum_{l=0}^{N} \tilde{\omega}_l a_j P_l(\mu_i) P_l(\mu_j). \tag{A2}$$

Substituting Eq. (A2) into (A1), we have

$$\mu_i \frac{dI(\tau,\mu_i)}{d\tau} = I(\tau,\mu_i) - \sum_j C_{ij} I(\tau,\mu_j). \tag{A3}$$

Eq. (A3) admits solutions of the form

$$I(\tau,\mu_i) = g_i \exp(-k\tau), \tag{A4}$$

where g_i are certain constants. Let us further define

$$b_{ij} = \begin{cases} C_{ij}/\mu_i, & \text{for } i \neq j \\ (C_{ij}-1)/\mu_i, & \text{for } i = j \end{cases} \tag{A5}$$

On the basis of Eqs. (A4) and (A5), the differential equations finally become

$$k g_i - \sum_j b_{ij} g_j = 0. \tag{A6}$$

Hence, the characteristic polynomial of the above set of linear equations is

$$f(k) = \begin{vmatrix} (k-b_{11}) & -b_{12} & \cdots & -b_{1n} \\ -b_{21} & (k-b_{22}) & \cdots & -b_{2n} \\ \vdots & \vdots & & \vdots \\ -b_{n1} & -b_{n2} & \cdots & (k-b_{nn}) \end{vmatrix} = k^n + d_1 k^{n-1} + d_2 k^{n-2} + \cdots + d_n = 0, \tag{A7}$$

where the coefficients can be obtained from

$$\left.\begin{aligned} d_1 &= -S_1 \\ d_2 &= -\tfrac{1}{2}(d_1 S_1 + S_2) \\ &\vdots \\ d_n &= -\frac{1}{n}(d_{n-1} S_1 + d_{n-2} S_2 + \cdots + S_n) \end{aligned}\right\}, \tag{A8}$$

with

$$S_n = \text{trace}\mathbf{B}^n. \tag{A9}$$

The matrix $\mathbf{B}$ is defined by

$$\mathbf{B} = \begin{bmatrix} b_{11} & b_{12} & \cdots & b_{1n} \\ b_{21} & b_{22} & \cdots & b_{2n} \\ \vdots & \vdots & & \vdots \\ b_{n1} & b_{n2} & \cdots & b_{nn} \end{bmatrix}. \tag{A10}$$

REFERENCES

Atwater, M. A., 1971: Radiative effects of pollutants in the atmospheric boundary layer. *J. Atmos. Sci.*, **28**, 1367–1373.

Bellman, R., H. Kagiwada, R. Kalaba and S. Veno, 1966: Nuerical results for Chandrasekhar's X and Y functions of radiative transfer. *J. Quant. Spectros. Radiat. Transfer*, **6**, 479–500.

Braslau, N., and J. V. Dave, 1973: Effect of aerosols on the transfer of solar energy through realistic model atmospheres. Part II: Partly-absorbing aerosols. *J. Appl. Meteor.*, **12**, 616–619.

Chandrasekhar, S., 1950: *Radiative Transfer*. New York, Dover, 393 pp.

Coulson, K. L., J. V. Dave and Z. Sekera, 1960: *Tables Related to Radiation Emerging from a Planetary Atmosphere with Rayleigh Scattering*. Berkeley and Los Angeles, University of California Press, 548 pp.

Danielson, R. E., D. R. Moore and H. C. van de Hulst, 1969: The transfer of visible radiation through clouds. *J. Atmos. Sci.*, **26**, 1078–1087.

Dave, J. V., 1970: Intensity and polarization of the radiation emerging from a plane-parallel atmosphere containing monodispersed aerosols. *Appl. Opt.*, **9**, 2673–2684.

Deirmendjian, D., 1969: *Electromagnetic Scattering on Spherical Polydispersions*. New York, Elsevier, 290 pp.

Dutton, J. A., and D. R. Johnson, 1967: The theory of available potential energy and a variational approach to atmospheric energetics. *Advances in Geophysics*, Vol. 12, New York, Academic Press, 445 pp.

Handbook of Geophysics, 1960: New York, The Macmillan Company, Chap. 16.

Hansen, J. E., 1969: Exact and approximate solutions for multiple scattering by cloudy and hazy planetary atmospheres. *J. Atmos. Sci.*, **26**, 478–487.

——, 1971a: Multiple scattering of polarized light in planetary atmospheres. Part I: The doubling method. *J. Atmos. Sci.*, **28**, 120–125.

——, 1971b: Multiple scattering of polarized light in planetary atmosphere. Part II: Sunlight reflected by terrestrial water clouds. *J Atmos. Sci.*, **28**, 1400–1426.

Herman, B. J., and S. R. Browning, 1965: A numerical solution to the equation of radiative transfer. *J. Atmos. Sci.*, **22**, 559–566.

——, —— and R. J. Current, 1971: The effect of atmospheric aerosols on scattered sunlight. *J. Atmos. Sci.*, **28**, 419–428.

Holland, A. C., and G. Gagne, 1970: The scattering of polarized light by polydisperse system of irregular particles. *Appl. Opt.*, **9**, 1113–1121.

Hovenier, J. W., 1969: Symmetry relationships for scattering of polarized light in a slab of randomly oriented particles. *J. Atmos. Sci.*, **26**, 488–499.

——, 1971: Multiple scattering of polarized light in planetary atmospheres. *Astron. Astrophys.*, **13**, 7–29.

Howell, H. B., and H. Jacobowitz, 1970: Matrix method applied to the multiple scattering of polarized light. *J. Atmos. Sci.*, **27**, 1195–1206.

Hunt, G. E., and I. D. Grant, 1969: Discrete space theory of radiative transfer and its application to problems in planetary atmospheres. *J. Atmos. Sci.*, **26**, 963–972.

Irvine, W. M., 1968: Multiple scattering by large particles. II. Optically thick layers. *Astrophys. J.*, **152**, 823–834.

——, and J. B. Pollack, 1968: Infrared optical properties of water and ice spheres. *Icarus*, **8**, 324–360.

Junge, C. E., 1963: *Air Chemistry and Radioactivity*. New York, Academic Press, 382 pp.

Keller, H. B., 1958: Approximate solution of transport problems. Part I. Steady-state, elastic scattering in plane and spherical geometry. *J. Soc. Ind. Appl. Math.*, **6**, 452–465.

——, 1960a: Approximate solution of transport problems. Part II. Convergence and applications of the discrete-ordinate method. *J. Soc. Ind. Appl. Math.*, **8**, 43–73.

——, 1960b: On the pointwise convergence of the discrete-ordinate method. *J. Soc. Ind. Appl. Math.*, **8**, 560–567.

Lenoble, J., 1956: Application de la méthode de Chandrasekhar à l'étude du rayonnement diffusé dans le brouillard et dans la mer. *Rev. Opt.*, **35**, 1–17.

Liou, K. N., 1973: Transfer of solar irradiance through cirrus cloud layers. *J. Geophys. Res.*, **78** 1409–1418.

——, and J. E. Hansen, 1971: Intensity and polarization for single scattering by polydisperse spheres. A comparison of ray optics and Mie theory. *J. Atmos. Sci.*, **28**, 995–1104.

——, and R. M. Schotland, 1971: Multiple backscattering and depolarization from water clouds for a pulsed lidar system. *J. Atmos. Sci.*, **28**, 772–784.

McElroy, M. B., 1971: The composition of planetary atmosphere. *J. Quant. Spectros. Radiat. Transfer*, **11**, 813–825.

Piotrowski, S., 1956: Asymptotic case of the diffuse of light through an optically thick scattering layer. *Acta Astron.*, **6**, 61–73.

Plass, G. N., and G. W. Kattawar, 1971: Radiance and polarization of the earth's atmosphere with haze and clouds. *J. Atmos. Sci.*, **28**, 1187–1198.

Samuelson, R. E., 1967: The transfer of thermal infrared radiation in cloudy planetary atmospheres. Ph.D. thesis, Georgetown University, 309 pp.

——, 1969: The thermal radiation field emitted by anisotropically scattering cloudy planetary atmospheres. *Icarus*, **10**, 258–273.

——, 1970: Non-local thermodynamic equilibrium in cloudy planetary atmospheres. *J. Atmos. Sci.*, **27**, 711–720.

Sekara, Z., 1956: Recent developments in the study of the polarization of sky light. *Advances in Geophysics*, Vol. 3, New York, Academic Press, 378 pp.

Shettle, E. P., and J. A. Weinman, 1970: The transfer of solar irradiance through inhomogeneous turbid atmosphere evaluated by Eddington's approximation. *J. Atmos. Sci.*, **27**, 1048–1055.

Stratton, J. A., 1941: *Electromagnetic Theory*. New York, McGraw-Hill, 415 pp.

Twomey, S., H. Jacobowitz and H. B. Howell, 1966: Matrix methods for multiple scattering problems. *J. Atmos. Sci.*, **23**, 289–296.

van de Hulst, H. C., 1963: A new look at multiple scattering. Tech. Rept., Goddard Institute for Space Studies, NASA, New York, 81 pp.

——, and K. Grossman, 1968: Multiple light scattering in planetary atmospheres. *The Atmospheres of Venus and Mars*, New York, Gordon and Breach, 288 pp.

Volz, F. E., 1971: Infrared absorption by atmospheric aerosol substances. *J. Geophys. Res.*, **77**, 1017–1031.

Waggoner, A. P., N. C. Ahlquist and R. J. Charlson, 1972: Measurement of aerosol total scatter-backscatter ratio. *Appl. Opt.*, **11**, 2886–2889.

Weinman, J. A., and P. J. Guetter, 1972: Penetration of solar irradiances through the atmosphere and plant canopies. *J. Appl. Meteor.*, **11**, 136–140.

Yamamoto, G., M. Tanaka and K. Kamitani, 1966: Radiative transfer in water clouds in the 10-micron window region. *J. Atmos. Sci.*, **23**, 305–313.

——, ——, and S. Asano, 1971: Radiative heat transfer in water clouds by infrared radiation. *J. Quant. Spectros. Radiat. Transfer*, **11**, 697–708.